UNIVERSITY OF AUCKLAND

MASTER'S THESIS

Modelling Comparison of a Geothermal Vaporiser: A Step Towards a Digital Shadow

Author: Theo BREHMER-HINE

A thesis submitted in fulfilment of the requirements for the degree of Master of Engineering

in the

Department of Chemical and Materials Engineering

in collaboration with

Project Ahuora - Centre for Smart Energy Systems

September 12, 2022

Declaration of Authorship

I, Theo BREHMER-HINE, declare that this thesis titled, "Modelling Comparison of a Geothermal Vaporiser: A Step Towards a Digital Shadow" and the work presented in it are my own. I confirm that:

- This work was done wholly or mainly while in candidature for a research degree at this University.
- Where I have consulted the published work of others, this is always clearly attributed.
- I have acknowledged all main sources of help.
- Where the thesis is based on work done by myself jointly with others, I have made clear exactly what was done by others and what I have contributed myself.

Signed:

_____

Date:

_____

Modelling Comparison of a Geothermal Vaporiser: A Step Towards a Digital Shadow

Theo BREHMER-HINE

ABSTRACT

New Zealand is experiencing the need to meet net-zero GHG emissions and growing energy demands. A key aim of the Ahuora research programme, that this work is contributing to, is the development of tools such as Digital Twins to decarbonise New Zealand's process heat sector and expand energy generation capabilities. The organic Rankine cycle (ORC) is a thermodynamic process capable of utilising low-temperature heat sources such as geothermal reservoirs and waste heat to generate power.

This thesis investigates the dynamic modelling of vaporisers in ORC systems to support the development and understanding of Digital Twins for New Zealand industries. Its focus is the dynamic modelling of an industrial scale geothermal vaporiser where a model developed using Aspen HYSYS and a First Principles model developed using Python were compared using various metrics. In terms of Digital Twin model fidelity, the Python model and Aspen HYSYS model would be categorised as a 3-2-1D model in the behaves-like, looks-like and connects-to attributes. In performance, good agreement between the temperature predictions was shown for outlet geothermal brine, vapour and working fluid of the Aspen HYSYS model with a percent error of 0.02%, 0.06% and 0.04%, respectively, for the validation case. The Python model showed a percent error of 0.69%, 2.37% and 0.003%, respectively, for the validation case. In comparing the ease of use of these software tools, a trade-off would need to be made in deciding which modelling software to use, weighing the monetary investment of using Aspen HYSYS and its high level of quality assurance against the time investment of using Python.

The First Principles model will be used to aid in development of a vaporiser model in the Ahuora platform.

Acknowledgements

First and foremost, I am extremely grateful to my supervisors Prof. Brent Young and Dr. Wei Yu. Without their invaluable guidance, feedback and patience, this work would not be complete. Additionally, this endeavour would not have been possible without support from the Ahuora research programme, to whom I am deeply indebted.

I would like to extend my sincere thanks to Dr. Robert Kirkpatrick for his practical advice and high level of expertise that he has generously shared.

Many thanks to Isaac Severinsen for his technical support and modelling guidance which has kept me on track numerous times.

To Fabian Hanik and Ray Robinson of Top Energy, I am very grateful for your time and supplying data from the Ngawha Geothermal power plant, which was integral to this work.

I am extremely grateful to my parents Robin Brehmer and Peter Hine for their continuing support. In particular Robin who has assisted me in the final edits of this work. Without her help, this work would be far less polished.

Thanks should also go to my partner for her support and belief in me that has kept me motivated during this project.

Last but not least, all my family and friends for their encouragement, company and support throughout this project.

Contents

Declaration of Authorship **iii**

Abstract **v**

List of Symbols **xvii**

1 Introduction **1**

1.1 Preface 1

1.2 Evaporators in the Primary Manufacturing Industry 2

1.2.1 Dairy Processing in New Zealand 2

1.2.2 Pulp and Paper in New Zealand 2

1.3 The Organic Rankine Cycle 3

1.3.1 ORCs in Waste Heat Recovery 3

1.3.2 Geothermal ORCs in New Zealand 3

1.4 Digital Twins 4

1.5 Project Aims and Objectives 5

1.5.1 Research Aims 5

1.5.2 Research Objectives 6

1.6 Thesis Outline 6

2 Literature Review **7**

2.1 Preface 7

2.2 ORC Configurations 7

2.2.1 Pre-heaters 8

2.2.2 Recuperators 8

2.2.3 Thermal Interface Loop 9

2.2.4 Dual Pressure ORC 10

2.2.5 Vaporisers Utilised with ORC Technologies 10

2.3 Modelling Overview 11

2.4 First Principles Modelling 12
2.4.1 Heat Transfer Paradigm 12
2.4.1.1 The Temperature Difference Method 12
2.4.1.2 The Log Mean Temperature Difference Method 12
2.4.1.3 The Number of Transfer Units (NTU) Method 13
2.4.2 Spatial Model Paradigm 13
2.4.2.1 The Lumped Method 14
2.4.2.2 The Moving Boundary Method 14
2.4.2.3 The Discretised Method 15
2.4.2.4 Two-Volume Method 16
2.4.3 Published Work Summary 16
2.4.3.1 Model Fidelity 17
2.4.3.2 Model Summary 18
2.5 Black Box Modelling 22
2.5.1 Linear Modelling Techniques 23
2.5.2 Nonlinear Modelling Techniques 23
2.5.2.1 Artificial Neural Networks Model 23
2.5.2.2 Fuzzy Logic Based Model 24
2.5.2.3 Neuro Fuzzy Modelling 24
2.5.3 Published Work Summary 24
2.5.3.1 Model Fidelity 25
2.5.3.2 Model Summary 25
2.6 Comparing First Principles and Black Box Models 28
2.7 Grey Box Models 29
2.8 Conclusions 29

3 Case Study **31**
3.1 Preface 31
3.2 System Description 31
3.3 Production Delivery System 32
3.4 Plant Description 32
3.4.1 Vaporiser Configuration 34
3.5 Geothermal Fluid Composition 34
3.6 Conclusions 35

4 Vaporiser and Plant Modelling **37**
4.1 Preface . . . 37
4.2 Aspen HYSYS Model . . . 37
4.2.1 Modelling Procedure . . . 39
4.2.2 Heat Transfer Coefficients . . . 39
4.2.3 Equations of State . . . 41
4.2.4 Model Specifications . . . 43
4.2.5 Approximating Working Fluid Flow-rate . . . 43
4.2.6 Model Tuning . . . 44
4.2.7 Steady State Model Validation . . . 44
4.3 First Principles Model . . . 46
4.3.1 Software . . . 46
4.3.2 Model Formulation . . . 46
4.3.3 Cross-flow Configuration . . . 47
4.3.4 Heat Transfer Coefficients . . . 47
4.3.5 Equations of State . . . 48
4.3.6 Data-Driven Correlations . . . 48
4.3.6.1 Temperature and Density Curves . . . 49
4.3.6.2 Validation of Curves . . . 55
4.3.7 Model Tuning and Steady State Validation . . . 55
4.4 Dynamic Comparison . . . 56
4.4.1 Working Fluid Step Change . . . 58
4.4.2 Brine Step Change . . . 59
4.5 Conclusions . . . 59

5 Model Comparison **61**
5.1 Preface . . . 61
5.2 Comparison Criteria . . . 61
5.2.1 Performance . . . 61
5.2.2 Availability . . . 62
5.2.3 Ease of Use . . . 62
5.2.4 Model Fidelity . . . 63
5.3 Conclusions . . . 65

6 Conclusions **67**

6.1 Future Work 68

7 Appendices **71**

Appendix A: Working Fluid Fitted Correlations 71

Appendix B: Geothermal Fluid Fitted Correlations 75

Appendix C: First Principles Paper Summary 76

Appendix D: Black Box Paper Summary 78

List of Figures

2.1 Diagram of a basic ORC configuration 7
2.2 Diagram of an ORC configuration including a pre-heater 8
2.3 Diagram of an ORC configuration including a recuperator 9
2.4 Diagram of an ORC configuration including a thermal interface loop . 9
2.5 Diagram of a dual pressure ORC configuration 10
2.6 The Lumped modelling method diagram 14
2.7 The Moving Boundary method where Qsub, Qsat and Qsup refer to the subcooled, saturated and superheated regions of the working fluid. 15
2.8 The Discretised modelling method with (n) number of discretised cells 15
2.9 Graphical display of model purposes of the First Principles papers found 16
2.10 Graphical display of software used in First Principles model development 17

3.1 A simplified process flow diagram of the working fluid cycle of the Ngawha OEC4 plant 33
3.2 The vaporiser shell and tube configuration for Ngawha OEC4 plant . . 34

4.1 Aspen HYSYS schematic of plant and vaporiser model. Specified stream conditions are noted in tables. 38
4.2 The Aspen HYSYS schematic of the vaporiser model. The Vap - Brine and Vap - Steam refer to the brine and geothermal steam of the vaporiser. 39
4.3 Configuration of the First Principles model with a discretisation of seven 48
4.4 Prediction of temperature in (°C) in Figure A and density in kgm^{-3} in Figure B of n-pentane. Both correlations are in terms of enthalpy and pressure 51

4.5 Prediction of temperature in (°C) in Figure A and density in kgm^{-3} in Figure B of the geothermal vapour. Both correlations are in terms of normalised enthalpy and pressure 53
4.6 Prediction of temperature in (°C) in Figure A and density in kgm^{-3} in Figure B of the geothermal brine. Both correlations are in terms of normalised enthalpy and pressure 54
4.7 Step change of the working fluid (A) and brine (B) flow-rates and the temperature response of the vaporiser for the Aspen HYSYS model and the First Principles model 57

7.1 Bubble point curve of the working fluid fitted against pressure 72
7.2 Dew point curve of the working fluid fitted against pressure 73
7.3 Saturated temperature curve of the working fluid fitted against pressure 74

List of Tables

3.1 Table describing the plant readings. The working fluid flow-rate and turbine efficiency are approximated 32
3.2 The composition of simplified geothermal vapour 35

4.1 Comparison of Equations of State in calculating the saturation pressure and NCG mass flow-rate of the plant model 42
4.2 Optimised working fluid mass flow-rate for Case 1 and 2 44
4.3 Steady state results of plant and vaporiser of Case 1 44
4.4 Steady state results of plant and vaporiser of Case 2 45
4.5 Validation of data-driven correlations against data generated from Aspen HYSYS 55
4.6 Steady state validation of FP model against plant data from Case 1 . . 56
4.7 Steady state validation of FP model against plant data from Case 2 . . 56
4.8 Working fluid step change - Dynamic comparison between Aspen HYSYS model and FP model 58
4.9 Brine step change - Dynamic comparison between Aspen HYSYS model and FP model 59

5.1 Error of the Aspen HYSYS vaporiser model for steady state Case 1 and 2 62
5.2 Error of the First Principles vaporiser model for steady state Case 1 and 2 62
5.3 Summary of the comparisons of the First Principles and Aspen HYSYS model attributes 64

7.1 First Principles paper summary where MD and MS stand for Modelica Dymola, and MATLAB Simulink environments respectively. NA is used where no validation data or software is provided 76
7.2 Black Box paper summary where NA is used shown when no validation data or software is provided 78

List of Symbols

A	surface area	m^2
C_p	specific heat	$J/kg^\circ C$
d	diameter	m
f	friction factor	-
h	convective heat transfer coefficient	$W/m^2{}^\circ C$
H	mass enthalpy	$J\,kg^{-1}$
L	length	m
$\dot{m}$	mass flowrate	$kg\,s^{-1}$
M_w	molecular mass	$g\,mol^{-1}$
N_t	number of tubes	-
Nu	Nusselt number	-
P	pressure	bar
P_r	reduced pressure	-
Pr	Prantl number	-
Q	heat flow	W
Q_{flux}	heat flux	$W\,m^{-2}$
Re	Reynolds number	-
Rp	relative roughness	-
T	temperature	$^\circ C$
t	time	s
U	overall heat transfer coefficient	$W/m^2{}^\circ C$
V	volume	m^3
x	vapour fraction	-
X_{tt}	Lockhart-Martinelli parameter	m^3
z	length down tube	m
ρ	density	$kg\,m^{-3}$
η	efficiency	

μ	viscosity	Pa s
ε	absolute roughness	m

Subscripts

wf	working fluid
gf	geothermal fluid
v	geothermal vapour
l	geothermal brine
w	tube wall
o	outer
i	inner
vap	vaporiser
ncg	non-condensable gas preheater
out	outlet
in	inlet
n	normalised
gen	generated

Chapter 1

Introduction

1.1 Preface

In order to meet New Zealand's goal of net-zero greenhouse gas (GHG) emissions by 2050, development into disruptive decarbonisation technologies in the process heat sector will be required. In 2016, the energy sector reported 39.8% of New Zealand's total GHG emissions, 28% of which are related to process heat. This equates to 8.3 million tonnes of carbon dioxide (EECA, 2019). These emissions related to process heat are mostly (79%) a result of domestic manufacturing industries which encompass the pulp and paper, food and beverage manufacturing, petrochemical, and chemical processing industries

A key unit operation used in the food and beverage industry, and the pulp and paper industry is the evaporator. In pulp and paper, evaporation is used to re-concentrate black liquor to be reused in the process. Evaporation plants in paper mills have been shown to account for 24-30% of the mill's total energy requirement (Kumar, Kumar, and Singh, 2013). In the food and beverage industry evaporation is used in multiple applications such as a pre-concentration step before spray drying in the production of milk powder products, in the concentration of fruit juices and in the crystallisation of sugar.

Another application of evaporators in the energy generation industry is as an essential part of the Organic Rankine Cycle (ORC). In this context a vaporiser is the more commonly used terminology. ORC technology utilises low enthalpy sources in energy generation which has been applied in waste heat recovery (WHR), binary geothermal plants, biomass combustion plants and solar thermal plants (Meyer et al., 2013). As evaporators and vaporisers are essential to New Zealand industry, optimisation of this technology will assist in reducing emissions related to New

Zealand's process heat sector.

This thesis is a part of the Ahuora research programme which focuses on developing and integrating technology in the form of Digital Twins to aid the decarbonisation of the process heat sector while also expanding energy generation of New Zealand's energy resources. Investigation into various models of evaporators and ORCs was conducted to inform modelling best practices. This can be broadly categorised into First Principles, Black Box and Grey Box modelling.

1.2 Evaporators in the Primary Manufacturing Industry

Evaporation plays a vital role in the manufacturing industry as it allows the removal of water and concentration of the product. The largest users of this technology include the dairy manufacturing industry and the pulp and paper industry which collectively generated 44% of the revenue of the primary manufacturing sector in 2020 (Ministry for Primary Industries, 2020).

1.2.1 Dairy Processing in New Zealand

New Zealand's dairy industry makes up a key part of the primary manufacturing industry, generating NZ$20 billion in revenue for the year-end June 2020. New Zealand leads the world in global exports of whole milk powder at 1.5 million tones of whole milk powder in 2019, and in the same year exports 373 thousand tonnes of skim milk powder. Other major exports include cheese, butter and other protein products such as whey protein powder (USDA, 2020; Ministry for Primary Industries, 2020).

1.2.2 Pulp and Paper in New Zealand

The New Zealand Pulp and Paper industry generated NZ$646 million from pulp and NZ$492 million from paper and paperboard products in 2020 (Ministry for Primary Industries, 2020). An integral part of producing pulp and paper products is pulping which separates the wood fibres: this can be achieved through mechanical or chemical pulping. Chemical pulping yields a lower amount of fibres, however, the product has improved strength properties when compared with mechanical pulping. In chemical pulp mills such as Kraft and Soda pulp mills, there is a recovery of

spent cooking chemicals used in the chemical pulping process. These spent chemicals are called weak black liquor. Weak black liquor is recovered and concentrated through evaporation from 12-14% to 40-55% solids (Bajpai, 2018; Yadav and Verma, 2020).

1.3 The Organic Rankine Cycle

The organic Rankine cycle is based on the Rankine cycle, a heat engine cycle which converts heat into work through a four-step process: adiabatic compression, isobaric heating, adiabatic expansion and isobaric cooling. This thesis will focus on the modelling of the heating stage where the working fluid is vaporised in a vaporiser. How ORCs differ from the Rankine cycle is in the use of a working fluid as an alternative to steam. Use of a working fluid with a boiling point lower than water allows extraction of heat from lower temperature and enthalpy sources (Lie, 2015; Pethurajan, Sivan, and Joy, 2018; Southon, 2015). The selection of this working fluid is determined by the conditions of the application. This has been applied to medium temperature geothermal fluids, the waste heat of industrial processes, combustion of biomass and concentrated solar energy (Lie, 2015; Pethurajan, Sivan, and Joy, 2018; Southon, 2015).

1.3.1 ORCs in Waste Heat Recovery

Waste heat refers to unused heat generated from a thermal process that would be directly vented or exhausted to the environment. Venting of heat is prevalent in New Zealand manufacturing industries such as the food and beverage processing industry, pulp and paper industry, petrochemical industry, and metal production industry. In ORC applications waste heat is used to heat and evaporate the working fluid from where this energy is then extracted. Investigations have found that low-grade waste heat accounts for 50% of the total heat generated in the industry, therefore recovery of this waste heat can provide economic and environmental incentives (Dong, 2020; Hung, Shai, and Wang, 1997; Lie, 2015).

1.3.2 Geothermal ORCs in New Zealand

ORC technology is also utilised in obtaining power from medium temperature geothermal reservoirs, where the geothermal fluid is used to heat the working fluid. Energy

is generated from passing the vaporised working fluid through a turbine. This is referred to as a binary plant as two separate fluids are used (DiPippo, 2005a; Dong, 2020; Lie, 2015). Geothermal plants currently installed in New Zealand have the capacity to generate 1028 MW, with binary geothermal plants accounting for 186 MW of this (Lawless, Campen, and Randle, 2020). Overall, geothermal power plants produce 18% of New Zealand's energy (Pan et al., 2019; Ministry of Business, Innovation and Employment, 2021).

1.4 Digital Twins

A Digital Twin (DT) in a manufacturing context consists of a virtual representation of a production system. A DT is able to run simultaneously with the physical system, whereby, an automatic and bi-directional connection of data flows between the physical and virtual systems. A role of the DT of manufacturing systems is to predict and optimise the behaviour of the system in real time. At lower levels of integration between model and system exist digital shadows and digital models. A digital shadow is where the automatic flow of data is uni-directional from the physical system to the virtual system, while a digital model has no automated flow of data between the systems (Kritzinger et al., 2018). A subtle adjustment to this classification was made by (Yu et al., 2022), where the term digital manager is used to describe a two-way connection. This distinction is made to encompass DTs used in plant design or plant retrofits rather than only plant control systems.

From Yu et al., 2022's review, a classification framework is proposed in order to categorise the fundamental attributes of a DT: these being behaves-like, looks-like, and as described above, the connected-to attribute. The behaves-like attribute is further categorised into single-state, discrete (multiple steady states) and dynamic. The looks-like attribute is further categorised into a 1-D representation (e.g. a process flow diagram), a 2-D representation (e.g. a process flow diagram with plant dimensions and coordinates) and a 3-D representation (e.g. a virtual or augmented reality plant model). The time-scale and physical-scale is also used in this classification framework. The fidelity requirements for each of the fundamental attributes of a DT is unique to the application. The requirements of the application also influence the software and the modelling basis used in DT development.

The first step in DT development is in building a digital model of a system. As such, an investigation was conducted into various models of evaporator and ORC systems. A significant portion of the models seen in literature have been developed using commercial process simulators such as Aspen Plus, Aspen HYSYS, VMG Symmetry, gProms and Modelica. Models developed using these software programs display a process flow diagram of this system itself and are capable of modelling both steady state and dynamic systems. This is similar to First Principles (FP) based models developed in software such as MATLAB, however, in FP models no visual representation of the system is typically shown. A significant amount of empirical (Black Box) models have also been developed for these systems in steady state and dynamics, however, these also lack visual representations. Of these models, only Soares et al., 2019 developed a model with a connection between the model and a system.

1.5 Project Aims and Objectives

1.5.1 Research Aims

The goal of the Ahuora research programme, is to develop a platform using novel Digital Twin technology in order to reach net-zero GHG emissions by 2050 in the process heat sector. This project coincides with aim 1 of project Ahuora: focusing on developing models to aid in the development of the Ahuora platform.

To address the gap in industrial scale models of geothermal applications, the Ngawha geothermal power plant's vaporiser will be the subject of this thesis. In this context, the term 'vaporiser' is used to describe this unit operation, and as such, this term will be used henceforth. Due to the absence of research directly comparing modelling techniques of industrial scale vaporisers, this thesis will focus on comparing aspects outlined in Section 1.5.2, of the different modelling methodologies and modelling tools employed. These models will be developed in a commercial process simulator and open-source software for variety in comparison. A plant model was developed to aid in vaporiser model development and in future research to act as a virtual plant in the development of a digital shadow.

1.5.2 Research Objectives

- To develop dynamic digital models which can replicate the behaviour of a vaporiser unit operation utilising different modelling approaches.
- To compare vaporiser models and modelling approaches against the four aspects:
  - Performance: How accurate and fast are the predictions made by the simulation?
  - Availability: How accessible is the software?
  - Ease of use: How difficult to use was each software platform?
  - Digital Twin Fidelity Framework: How would these models be categorised using this framework?

1.6 Thesis Outline

Chapter 2 of this thesis will cover a review of literature on the various types of ORC modelling methodologies to inform the common practices in model development. This will be followed by a description of the system itself in Chapter 3. Based on the investigation of Chapter 2, two methodologies will then be developed. The performance of these models will be compared under steady state and dynamic conditions in Chapter 4. In Chapter 5 the comparison will be extended to aspects of the modelling software stated in Section 1.5.2. In Chapter 6 the results will be summarised and recommendations given for improving and furthering the current work.

Chapter 2

Literature Review

2.1 Preface

This chapter covers an investigation into modelling vaporisers used in energy generation. First, we take a broad look into the background knowledge of ORC systems and then into the methodologies for modelling these vaporisers. This is followed by an in-depth review of the models produced in these papers.

2.2 ORC Configurations

As described previously, an ORC has four basic components: compression, isobaric vaporisation, isentropic expansion and finally isobaric condensation. This basic configuration is shown in Figure 2.1.

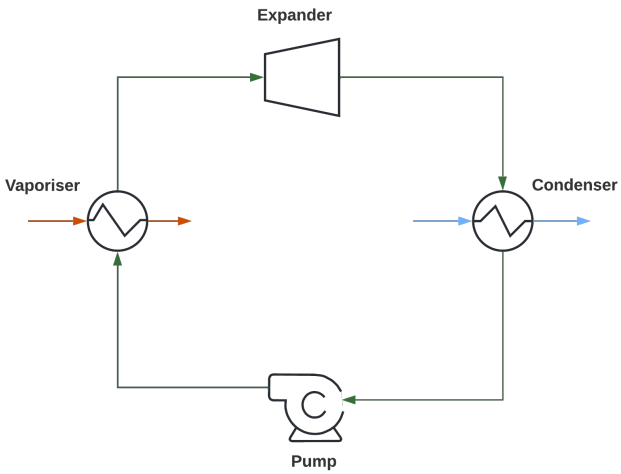

FIGURE 2.1: Diagram of a basic ORC configuration

Additionally, pre-heaters, recuperators, heat transfer loops and dual evaporators may be used to improve system efficiency, however, this is dependent on the parameters of the ORC system.

2.2.1 Pre-heaters

Pre-heaters can be used when an additional lower temperature heat source is available. Typically, in geothermal applications, this is reusing the main source through one or multiple additional heat exchangers. The additional heating before entering the vaporiser allows further extraction of enthalpy from the heat source. This increases the capacity of the working fluid of the system and therefore increases the power output (Lie, 2015). Figure 2.2 displays this configuration.

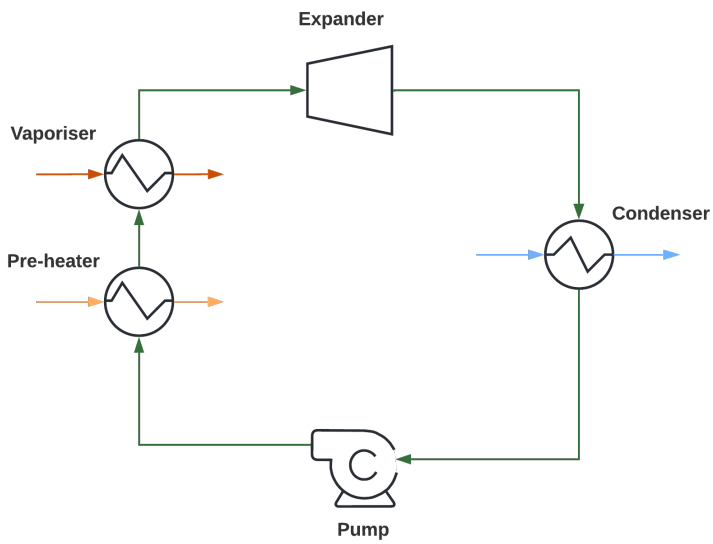

FIGURE 2.2: Diagram of an ORC configuration including a pre-heater

2.2.2 Recuperators

Recuperators can be used when the outlet from the expander remains superheated (Quoilin et al., 2013). This has the added benefit of recovering more enthalpy from the working fluid before it is condensed. This pre-heats the working fluid before the vaporiser. A recuperative cycle is shown in Figure 2.3.

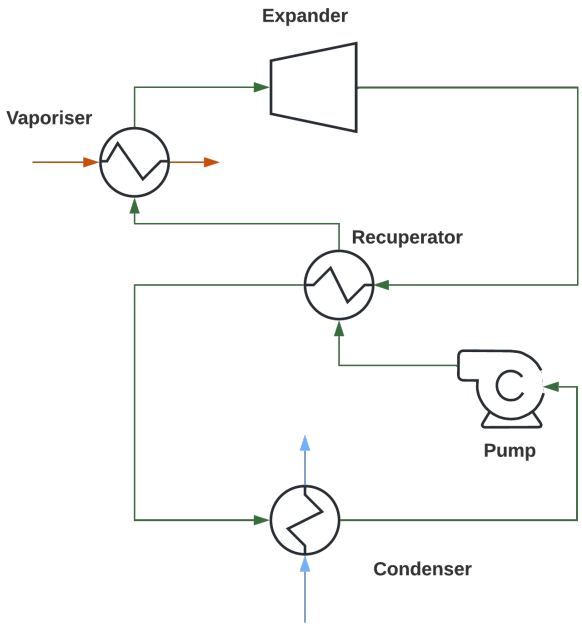

FIGURE 2.3: Diagram of an ORC configuration including a recuperator

2.2.3 Thermal Interface Loop

A thermal interface loop can be used to improve working longevity and provide a more stable operation with fluctuating heat sources (Meyer et al., 2013; Jiménez-Arreola et al., 2017). As a result, this configuration is typically used in a waste heat recovery application, as shown by (Zhao et al., 2018; Jiménez-Arreola et al., 2017). This configuration is shown in Figure 2.4.

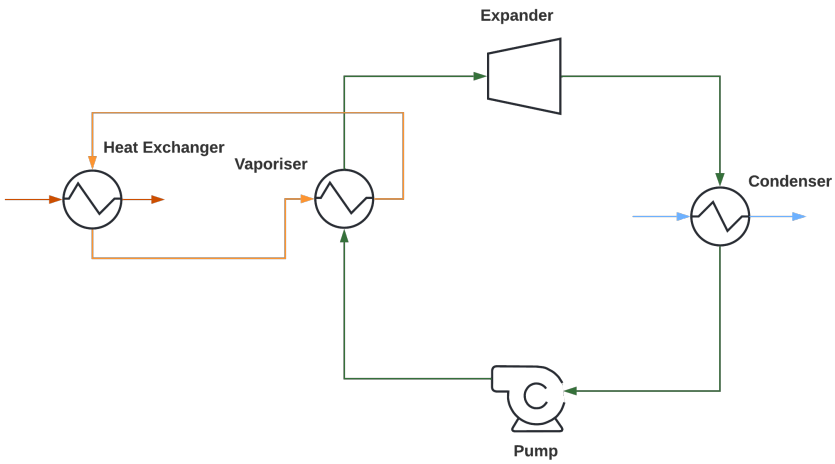

FIGURE 2.4: Diagram of an ORC configuration including a thermal interface loop

2.2.4 Dual Pressure ORC

A dual pressure ORC can be used under various configurations. Figure 2.5 replicates a configuration of a dual pressure geothermal ORC shown in (DiPippo, 2005b). This showed a higher utilisation efficiency when compared with a basic configuration cycle. Additionally, a dual-evaporator cycle in waste-heat recovery has also been shown in the literature (Seitz et al., 2016).

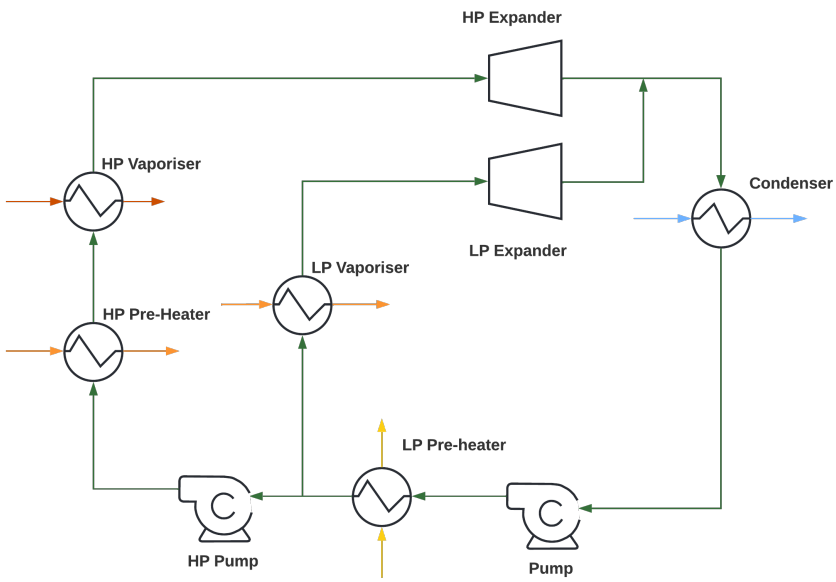

FIGURE 2.5: Diagram of a dual pressure ORC configuration

2.2.5 Vaporisers Utilised with ORC Technologies

The main types of heat exchangers utilised by industry in ORC applications are shell and tube heat exchangers, plate heat exchangers and finned tube heat exchangers. The most widely used of these are the shell and tube heat exchangers (Lie, 2015; Quoilin et al., 2011). A subset of this type of heat exchanger is the kettle reboiler, which is used in the vaporisation of the working fluid in large-scale geothermal binary plants. Here the working fluid is passed through the shell-side while the geothermal fluid or steam is passed through the tube-side (Lie, 2015; Proctor et al., 2016; Sun and Li, 2011). In smaller-scale applications, plate heat exchangers are used due to their compact size and higher heat transfer coefficient. In waste heat recovery of gases, finned tubular heat exchangers are typically utilised (Wang et al., 2017; Lie, 2015). Finned tubular heat exchangers allow the exhaust, which commonly has poor

convective heat transfer properties, to be passed shell-side, which improves heat transfer.

2.3 Modelling Overview

Modelling of processes allows for simulation and prediction of process behaviour which can be used for a variety of purposes. The model purpose or why the model is developed dictates the requirements of the model and, therefore, will have an impact on key development decisions. From the investigation into literature, the main purposes for model development are variable prediction, testing control strategies, comparing modelling methodologies, design optimisation and operational optimisation. The development of process models in predicting variables of a vaporiser is a key part of this thesis and is furthered by the comparison of the two separate modelling methods. These types of models can be broadly categorised into steady or dynamic states, and First Principles, Black Box and Grey Box models.

Steady state models are used when the dependent variables are static and therefore do not account for time. The main purpose behind steady state based models is in the prediction of key variables, design and optimisation of an ORC system (Proctor et al., 2016; Lie, 2015). Dynamic models describe the change in dependent variables as a function of time (Roffel, 2006). The use of a dynamic model of an ORC extends to testing control applications that can be used in improving control performance, exploring new options with respect to control, or design and dynamic optimisation (Georgiadis, Banga, and Pistikopoulos, 2011; Xu et al., 2020).

First Principles models are based on physical laws of conservation of mass, energy and momentum. These models are also referred to as mechanistic or white box. These types of models give physical insight into the processes occurring and typically, these models require significant time in development. Black Box or empirical models are based on input and output data: these models describe the relationship between these variables. Black Box models require data for which to train and validate the model and, typically require less time in development (Roffel, 2006). Another model type is the Grey Box or hybrid model which is developed using various structures of mechanistic and Black Box models (Sansana et al., 2021).

2.4 First Principles Modelling

In vaporisers, heat is transferred from the high-temperature fluid through a conductive material to a lower temperature fluid, with the intended effect of evaporating a product. Different methodologies have been developed in literature in order to model vaporisers. This section will cover First Principles (FP) models which focus on theoretical or physics-based models. Following, is an examination of FP modelling techniques. A sub-set of these models is process flow simulators where in-built unit operations are available in the software used.

2.4.1 Heat Transfer Paradigm

The heat transfer model describes the method of calculation of heat transfer between the vaporiser fluids. The main types of heat transfer modelling used throughout the literature were the temperature difference method, log-mean temperature difference method and NTU method. In addition to these methods, the enthalpy-based method is used, which considers the change in enthalpy of each fluid.

2.4.1.1 The Temperature Difference Method

This method calculates the heat transfer based on the temperature difference between two points. In a vaporiser, this is the temperature of the heating and product fluid. This temperature difference acts as the driving force for heat transfer. This is the most commonly used method in the literature for modelling a heat exchanger and has been used by Xu et al., 2020; Wei et al., 2008; Zhang et al., 2012. This relationship is shown by Equation 2.1.

$$Q = UA\Delta T \tag{2.1}$$

Where Q is the amount of heat transferred between two sides, U is the overall heat transfer coefficient, A is the transfer area and ΔT is the difference in temperatures.

2.4.1.2 The Log Mean Temperature Difference Method

The log-mean-temperature-difference (LMTD) method considers the LMTD between the two fluids as the driving force for heat transfer. This method is used in modelling counter-current heat exchangers. The addition of a geometrical term 'F' is used to

model different heat exchanger arrangements (Farid, 2010; Lie, 2015; Proctor et al., 2016). The LMTD method for heat transfer calculation is described by the following Equation 2.2, sourced from Farid, 2010.

$$Q = FU_{overall}A_{eff}\Delta T_{LMTD} \tag{2.2}$$

Where the F is the geometry factor, and the ΔT_{LMTD} is calculated by the following Equation 2.3.

$$\Delta T_{LMTD} = \frac{T_1 - T_2}{ln(\frac{T_1}{T_2})} \tag{2.3}$$

Where T_1 refers to the difference in temperatures of the fluids entering the heat exchanger and T_2 refers to the difference in temperatures of the fluids exiting the heat exchanger. This method is mainly used in steady state modelling such as in (Wang et al., 2013). However, this method is also applied in the dynamic model of a binary geothermal plant by Proctor et al., 2016, to model a shell and tube heat exchanger with multiple tube sets in VMG Symmetry.

2.4.1.3 The Number of Transfer Units (NTU) Method

The number of transfer units (NTU) method uses the heat exchanger efficiency, η, which is the ratio of actual heat transferred over the maximum heat transfer (Farid, 2010), shown below in Equation 2.4.

$$\eta = \frac{Q}{Q_{max}} \tag{2.4}$$

The NTU method is typically used when there is insufficient information to calculate the LMTD of the vaporiser (Lie, 2015). The NTU is calculated from the following Equation 2.5.

$$NTU = \frac{UA}{C_{min}} \tag{2.5}$$

Where C_{min} is the smallest value of thermal capacitance or (mC_p) of either the hot side or cold side. This method was used by Liu et al., 2017.

2.4.2 Spatial Model Paradigm

Another type of modelling paradigm used in the modelling of heat exchangers is the spatial paradigm. These modelling methods segment the heat exchanger along the

axial direction. Only the axial direction is considered, as incorporating other spatial dimensions may improve accuracy, however, it significantly increases processing requirements. The methods used for segmenting the heat exchanger include the lumped method, the moving boundary method, the discretised method and the two-volume method.

2.4.2.1 The Lumped Method

The Lumped Method is the simplest of the three methods as it does not account for the axial direction of flow. This method lumps the heat exchanger into a single point. In its simplest form, the heat capacities remain constant throughout the heat transfer length. This shows relative accuracy when no phase change occurs, however, this is not ideal for a vaporiser due to the change in physical properties. Although, accurate models have still been developed with additional tuning (Xu et al., 2020). This method has also been used by Wei et al., 2007; Feng et al., 2020. A diagram displaying this method is shown in Figure 2.6.

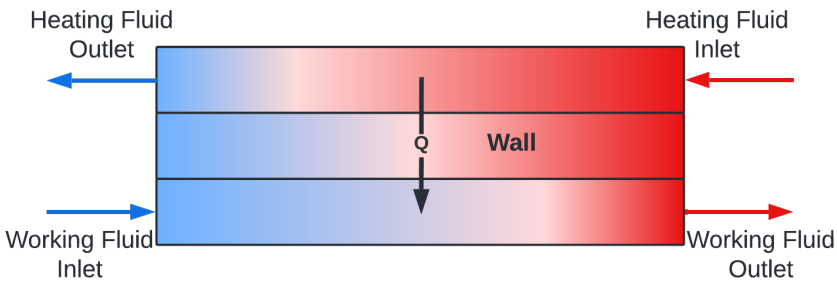

FIGURE 2.6: The Lumped modelling method diagram

2.4.2.2 The Moving Boundary Method

The Moving Boundary Method (MBM) is an intermediate between lumped analysis and the discretised method as it segments the heat transfer length into three separate regions of the working fluid's pipe flow. These regions correspond to the liquid phase region, the two-phase region and the vapour phase/superheated region. This method is suitable for vaporisers as this accounts for changes in the density, heat capacity and heat transfer coefficient of each region as a result of phase change. This method has been utilised by Xu et al., 2020; Huster et al., 2018; Sun and Li, 2011. A diagram displaying this method is shown in Figure 2.7. Though this phase-based

segmentation is shown applied only to the working fluid, it can also be applied to the heating fluid if it is condensing. This is common in geothermal applications where geothermal steam is condensed.

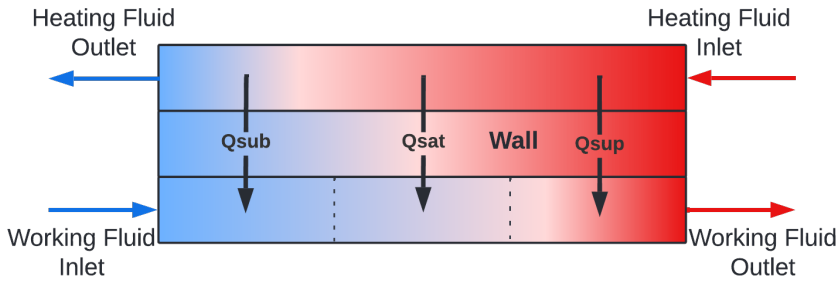

FIGURE 2.7: The Moving Boundary method where Qsub, Qsat and Qsup refer to the subcooled, saturated and superheated regions of the working fluid.

2.4.2.3 The Discretised Method

This method discretises the length along the vaporiser into segments. The number of segments can vary in each model and can be tailored to suit the model's purpose (Huster et al., 2018). In each segment the heat transfer is calculated. Discretised models tend to have higher computational requirements than MBM. However, discretising methods have shown to have higher prediction accuracy (Wei et al., 2008; Xu et al., 2020). A diagram displaying this method is shown in Figure 2.8.

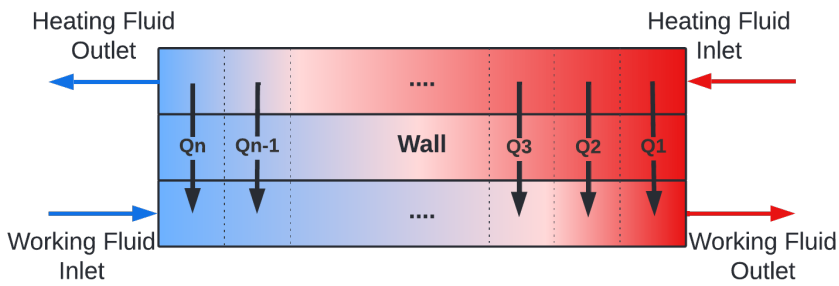

FIGURE 2.8: The Discretised modelling method with (n) number of discretised cells

Various studies have used this discretised method (Chowdhury et al., 2018; Xu et al., 2020; Wei et al., 2008). Several key decisions are made in development based on the model's purpose. These include the model's accuracy and the model's processing speed which inform which spatial paradigm suits the model's purpose.

2.4.2.4 Two-Volume Method

The Two-Volume method is newly developed and has been used only by (Pili, Spliethoff, and Wieland, 2017) in a geothermal binary vaporiser. This is suited to this application as the phase of the working fluid occurs in the shell-side of the heat exchanger, where a pool accumulates at the bottom of the shell (Imran et al., 2020; Pili, Spliethoff, and Wieland, 2017). This works through segmentation of the shell-side into a pool boiling and vapour region. In addition to this, the tube bundle was modelled through the discretised method described in Section 2.4.2.3. Mass balances are used for each region, where the condensation and evaporation rates are tuned based on experimental data.

2.4.3 Published Work Summary

The First Principles papers found are shown in Appendix C: First Principles Paper Summary. The industrial applications of the ORC models were waste heat recovery, geothermal binary systems, solar systems and bio-generation systems. Of the 57 papers found, 61% were waste heat recovery applications (WHR), followed by geothermal applications (Geo) at 23%. Biomass and solar applications comprise the remaining 16%. The purposes for developing these models have been identified as design, control applications, operational optimisation, variable prediction, modelling method comparison and novel method of modelling. The only novel method that was identified was shown by Pili et al., 2017. The model purpose of the FP papers found is shown in Figure 2.9. Steady state models comprise 82% and 36% of the 'Design' and 'Operational Optimisation' sections. The remaining papers were dynamic models.

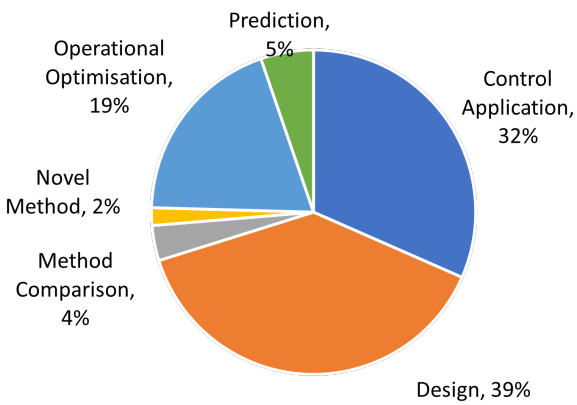

FIGURE 2.9: Graphical display of model purposes of the First Principles papers found

2.4.3.1 Model Fidelity

As described previously, the digital model fidelity is a categorisation framework used for Digital Twins based on the behaves-like, looks-like and the connects-to attributes. All of the above models require manual input of data from the physical system to the digital model, therefore would be classified as Digital Models.

The behaves-like attribute of the model is determined by the type of validation conducted for the model. Of the papers shown in Table 7.1, 44% made no mention of the source of their validation data. A majority (72%) of them were steady state models and therefore would be classified as 0-D in this respect. The other papers were validated against data generated from validated models, labs, pilot plants and industrial plants. Of the validated papers, 88% were found to be done so dynamically and therefore would be classified as 3-D fidelity for the behaves-like attribute. The remaining 12% which were steady state models include Hettiarachchi et al., 2007; Wang, Wu, and He, 2019; Khennich and Galanis, 2012; Altun and Kilic, 2020, all of which were validated against a single steady state case, and therefore would be classified as 1-D.

The looks-like attribute is largely determined by the software tool used in model development. There is likely to be only a visual representation when it is readily available in the software. The various software tools stated in the literature are shown in Figure 2.10. The software tools which do have a visual representation used in literature include Aspen Plus, Aspen HYSYS, VMGSim, gProms, GT Suite, MATLAB/Simulink, Modelica/Dymola and Simsci Pro II.

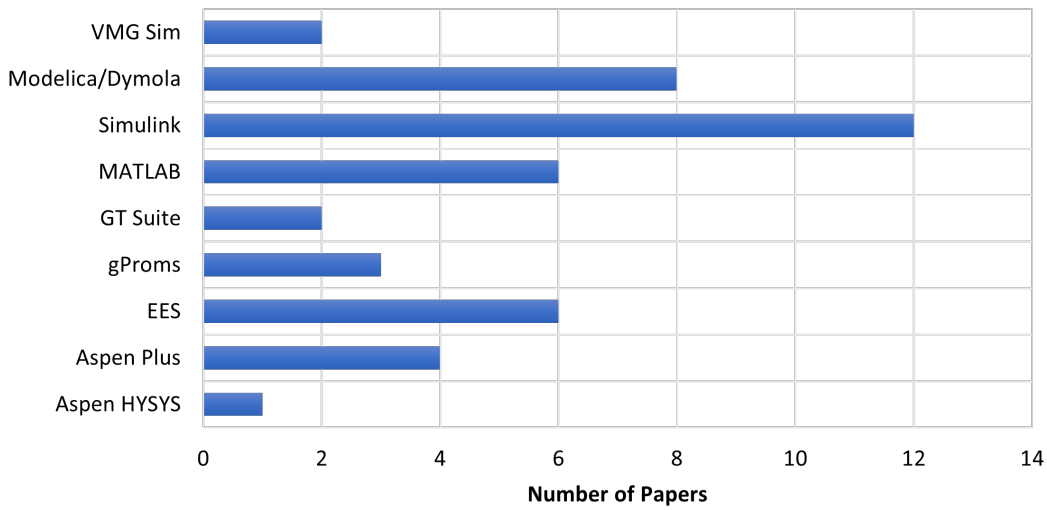

FIGURE 2.10: Graphical display of software used in First Principles model development

2.4.3.2 Model Summary

From the papers found on First Principles models, those produced since 2018 were further analysed. A summary of the models developed in these papers follows. This is used to summarise common practices and results of these FP models.

A model was developed of a WHR of an ORC by Xu et al., 2020. Three dynamic First Principles models were compared including: a lumped model, moving boundary model and discretised modelling method. Correction factors to the heat exchanger efficiency and heat transfer coefficient were used based on steady state experimental data, which were then optimised through particle swarm optimisation. A thermal inertia term was also used in slowing the change in enthalpy of the lumped model, which was optimised with MATLAB's grid search method. The accuracy and computational costs were compared. The lumped, MBM and 30 cell-discretised model required 4.6 s, 27.9 s and 118.6 s, respectively in simulating a 650 s test. All models had relatively low mean error percentages of below 1.5% and mean errors below 6.6K. The discretised model showed the highest prediction accuracy and required less development effort and time than the MB method. Each model can be used for a specific purpose based on its specific attributes.

A combined cooling-heating and power system from a geothermal source was modelled dynamically by Cao et al., 2021. The moving boundary method was used in the operational optimisation of this 250 kW ORC system to improve the controller performance of changing heating and cooling loads. MATLAB Simulink and REFPROP were used in developing the model. No details were provided on the prediction error of this system, however, predictions showed consistency through a graphical validation against data provided in the literature.

A steady state model was produced for comparing ORC configurations by Wang, Wu, and He, 2019. An enthalpy-based approach was taken in the design of this system. MATLAB and REFPROP were used in producing the model. Particle Swarm Optimisation was used in optimising the net power output of the model. This model was validated against data from previous literature showing a percent error of 0.49% and 0.5% for evaporation temperature and net power output. A Partial Evaporating dual-pressure ORC system was found to have the best thermal performance, with increased net power output and exergy efficiency up to 27% and 4.6% respectively.

A steady state model was produced for a binary power plant by Altun and Kilic,

2020. The enthalpy-based modelling methodology was used for the vaporiser. This model was produced using EES and validated against SCADA (Supervisory Control and Data Acquisition) data from a geothermal plant. The model was additionally validated against another binary geothermal plant. Minor differences were observed between both validations. This model was used to assess the feasibility of a recuperator. Optimal operational conditions were found under the configurations with and without the recuperator. With the proposed internal heat recovery system (recuperator), the power output increased by 15%.

A steady state model was produced in the optimisation and design of a waste heat ORC system by Feng et al., 2020. MATLAB and REFPROP were used in the optimisation of the enthalpy-based model. Results showed a maximum net power output of 37 kW, an increase of 25% from the previous power output.

Petrollese and Cocco, 2020 developed an approach for steady state modelling of solar-based ORC systems. Lumped analysis was used on the vaporiser. This model was used in the design of four case studies. Toluene as the working fluid was found to perform the best with the lowest levelised cost of ownership for all four cases.

Aspen HYSYS was used in the design and thermo-economic optimisation of a geothermal power plant by Hidayah, Putera, and Subiantoro, 2020. Comparison of basic and recuperative configurations and various working fluids were tested in these optimisations. N-pentane showed the best performance thermodynamically and economically, with a thermal efficiency of 15% and a specific investment cost of $4,300 per kW. The basic configuration showed better economic performance despite the recuperative configuration's better thermal efficiency. The payback period of the basic ORC system is one year shorter with lower specific investment costs.

A geothermal application was dynamically modelled by Pili et al., 2020 for controller improvement. This model was developed in a Dymola environment with REFPROP for access to thermodynamic properties. The plate heat exchanger was modelled using the discretised modelling approach. The ORC was validated against a test rig with a net power output of 5-10 kW. Predictions showed a relative root mean square error (RRMSE) of 1% and 0.4% for the working fluid and water outlets to the vaporiser.

Carraro et al., 2019 developed a dynamic simulation of a small-scale WHR ORC system with a net power output of 3.1 kW. The MB method was used in modelling a plate heat exchanger used as the vaporiser. This was developed in a MATLAB

Simulink environment in addition to REFPROP. In validation against the test rig, a maximum relative error of 1.4% for the vaporiser outlet temperature was shown.

A dynamic model was produced in order to compare direct and indirect evaporation utilising a thermal oil loop by Carraro et al., 2019. Plate, and shell and tube, vaporisers were used as the indirect vaporisers, while fin and tube were used as the direct vaporiser. These models were produced at the design stage in Dymola. As such, the components were based on validated models in the TIL library. Approximately 55 kW of thermal power was transferred into the ORC loop. Implementation of the thermal oil loops has the advantage of damping heat source fluctuations, although with the trade-off of a higher footprint and lower thermal efficiency.

An enthalpy-based model was produced in the design and optimisation of a micro-scale bio-generation CHP system by Wang, Wu, and He, 2019. This system had a net power output of 2.1 kW. The model was developed in MATLAB, using REFPROP and validated against available literature data (Jang and Lee, 2018). Relative errors of 0.3% and 1.4% were shown for the thermal efficiency and net power output of the model, respectively. The developed optimisation algorithm was tested and found the optimal power output and thermal power output to be 1.7 kW and 37 kW, respectively.

Zhang et al., 2019 developed a discretised dynamic model in Dymola. Experimental data from the test rig system was used in the validation of the models produced. Discrepancies were seen in the working fluid outlet of the vaporiser, with a 20% maximum relative error (MRE). A significantly better prediction was shown in the heating source outlet of the vaporiser with a MRE of 1.7%.

(Zhao et al., 2018) developed a model of a diesel engine-ORC combined system with a net power of 2.5 kW in GT-suite. This was integrated with Simulink in order to test the performance of control strategies. The shell and tube vaporiser was modelled and verified based on tutorials from GT-suite which recommend the deviation between the wall and working fluid temperature is less than 25%. This standard was met, however, no additional validation against experimental data was done for the vaporiser.

A steady state model was produced in MATLAB for a geothermal application utilising a recuperator and pre-heater by Sun, Liu, and Duan, 2018. A discretised LMTD heat exchanger method was used in modelling the shell and tube vaporiser. This model was used in optimising net power output through changing vaporiser

pinch temperature and heat exchange area. As the pinch point temperature difference (PPTD) decreased, the required area for heat exchange increased. At a brine inlet temperature of 150°C and a PPTD of 4°C, the optimal conditions found a net power output of 1900 kW.

An enthalpy-based model was produced to design and optimise a micro-scale combined heating and power system by Jang and Lee, 2018. The model was developed using EES. Various configurations and working fluids were tested. The optimal performance was found using cyclopentene as the working fluid and a recuperator in the configuration. This produced 2 kW net power.

A dynamic model of a solar ORC system capable of generating 16 kW net power was developed by Ni et al., 2018. The discretised modelling approach was used in modelling the shell and tube vaporiser in the Dymola environment. The model was developed for testing a PID control strategy. In validation against another study's experimental data (Fu, Lee, and Hsieh, 2015), a maximum relative error in outlet temperature of 2.1% and an average relative error of 0.96% were shown.

A dynamic model for a solar ORC system with thermal energy storage was developed by Li, Ma, and Li, 2018. The model was developed in the MATLAB/Simulink environment utilising the discretised approach. This model was used in determining the output power with solar disturbances and fluctuations.

A steady state model in Aspen Plus of a biomass ORC system using a thermal oil interface loop was developed by Nur and Sunoto, 2018. Configurations were tested with and without a recuperator where the exergy destruction was compared. No validation of the model was described in this paper. The recuperator was shown to decrease the exergy destruction by approximately 20 kW at ambient temperature conditions.

Bellos and Tzivanidis, 2018 developed a steady state model of a hybrid solar and waste heat ORC system. A lumped, enthalpy-based heat exchanger modelling method was used. Various working fluids were tested in order to maximise the heat source utilisation. Toluene as the working fluid performed the best, enabling the system to generate 480 kW to 850 kW when the waste heat source ranged from 150°C- 300°C, respectively.

Huster et al., 2018 developed a dynamic model of an ORC WHR system using gProms. The moving boundary approach was taken to model the vaporiser due to its lower computational requirements. As parameters were estimated based on

dynamic data, lower computational requirements were necessary. In validating the model against experimental data, the relative mean errors (RME) of the temperature of the working fluid and the exhaust gas leaving the vaporiser were 0.8% and 0.4% respectively. The relative maximum errors of these same streams were 2.7% and 1.2% respectively.

Other key research that was conducted prior to 2018 includes Pili, Spliethoff, and Wieland, 2017; Proctor et al., 2016.

As stated in Section 2.4.2.4, (Pili, Spliethoff, and Wieland, 2017) used a two-volume method in modelling a kettle re-boiler of a geothermal vaporiser. The dynamic model was produced in Dymola and the fluid properties were computed from REFPROP. The model was validated against a geothermal CHP plant, and both validation scenarios were predicted within 1% of the measured outlet temperature of the working fluid and brine.

(Proctor et al., 2016) produced a dynamic model in VMG Symmetry of a binary geothermal plant with a gross power generation of 10 MW. Due to the configuration of the vaporiser with multiple tube-sets, two coolers were used to model the heat transfer of each tube-set in addition to a heater modelling the heating of the shell side. The LMTD was calculated for each section which were multiplied by the static UA values. These UA values were calculated based on plant data. The resultant heat flow was summed and used for specifying the shell side heater. The average relative error was 1.7%, 5.0% and 3.2% for the working fluid, geothermal steam and geothermal brine, respectively.

2.5 Black Box Modelling

Black Box modelling or data-driven modelling involves fitting an equation relating a data-set of inputs to outputs. In process modelling, this involves treating the unit operation like a 'black box', taking the input data values and finding the relationship to the output data. In producing dynamic models these input values are the present values of the system while the output is the prediction of the future values. The main Black Box modelling techniques used in vaporiser modelling can be categorised into linear and non-linear modelling techniques.

2.5.1 Linear Modelling Techniques

Linear regression aims to fit a line to describe the relationship as an input and output. Auto-Regressive (AR) models are typically utilised in dynamic or time-dependent process modelling. An AR model uses previous output values of the time series in regression of future outputs, hence auto-regression (Ljung, 1998; Rhinehart, 2016). The addition of an X term represents the inclusion of exogenous variables, which is associated with the input in vaporiser modelling. Incorporating a moving average term which averages the most recent data values in a time series is shown by adding MA, (Rhinehart, 2016; Young, 1992). Equation 2.6 displays an Auto-Regressive Moving Average with Exogenous inputs model, more commonly referred to as an ARMAX model.

$$A(q^{-1})y(k) = B(q^{-1})u(k) + C(q^{-1})e(k) \tag{2.6}$$

Where $A(q^{-1})y(k)$ refers to the auto-regressive part, $C(q^{-1}e(k)$ refers to the moving average part and $B(q^{-1})u(k)$ refers to the exogenous variable.

2.5.2 Nonlinear Modelling Techniques

2.5.2.1 Artificial Neural Networks Model

Artificial neural networks are non-linear self-learning systems commonly applied in control methods and strategies. Neural networks consist of a number of layers, including the input and output layers which correspond to the input variables at the present time and the output variables predicted by the model. Between the input and output layers are the hidden layers which can vary in number. Each layer consists of several interconnected nodes or neurons. These neurons manipulate the input data or present values of the system to produce an output or prediction. Weights are applied to each connection and multiplied by the corresponding value of the connection. These values are summed together with a bias where if a threshold is met, set by an activation function, the neuron 'fires' and produces an output (Roffel, 2006).

Neural Networks come in various types and structures. The common structures seen in the literature include Feed Forward, Recurrent, Back-Propagation and Long Short-Term Memory. A Feed-Forward network represents the most basic network

structure and describes when particular, or multiple neurons connect to all the neurons in the following layer (Roffel, 2006; Palagi et al., 2019). A Recurrent network describes when a neuron is connected to neurons in a previous layer (Roffel, 2006; Palagi et al., 2019). A specific type of the Recurrent network is the Long Short-Term Memory or LSTM network which inputs not only the current time step's inputs but also an output from a previous time step (Roffel, 2006; Palagi et al., 2019). A Back-Propagation network uses the gradient of a defined cost or error function with respect to the weights of each modifiable connection. These weights are then updated to minimise the cost function (Roffel, 2006).

2.5.2.2 Fuzzy Logic Based Model

Fuzzy sets look to describe continuous domains of input and output variables by dividing the domains into a small number of overlapping regions, each having a corresponding linguistic value: for example high temperature, medium temperature or low temperature. The categorisation of the data or fuzzification occurs through membership functions (Roffel, 2006; Chowdhury, Nguyen, and Thornhill, 2015).

Based on the membership function value, a different linguistic term will be associated with this input. This linguistic term corresponds to a different mathematical relationship relating input to output. This type of fuzzy model is named the Takagi-Sugeno model. If, instead of a mathematical-based relationship, fuzzy reasoning is used, this is called a Mamdani model (Roffel, 2006).

2.5.2.3 Neuro Fuzzy Modelling

Neuro-Fuzzy modelling uses a neural network structure, which incorporates fuzzy characteristics of a Sugeno-type model to combine the advantages of both approaches (Roffel, 2006; Enayatollahi, Fussey, and Nguyen, 2020; Khosravi et al., 2019). This type of model is capable of learning non-linear mappings of data and has been used in both steady state and dynamic modelling of ORC units (Roffel, 2006; Enayatollahi, Fussey, and Nguyen, 2020; Khosravi et al., 2019).

2.5.3 Published Work Summary

The research papers using Black Box models are shown in Appendix D: Black Box Paper Summary. The applications of Black Box models researched in the literature include ORC models used in waste heat recovery, geothermal binary systems and

a hybrid solar and geothermal system by Khosravi et al., 2019. Of the 22 papers found, 86% were waste heat recovery applications, followed by 9% geothermal applications.

2.5.3.1 Model Fidelity

As in Section 2.4.3.1, the models seen in this area show no connection to their physical system, therefore, would be classified as digital models.

The behaves-like attribute of the model is determined by the type of validation conducted for the model. Of the validation seen in the literature, 91% of these models were validated against data generated from a validated model, lab or industrial plant. Of these models, 59% were steady state based models while 32% were dynamic models: these models would therefore be classified as 1-D and 3-D in the behaves-like attribute. None of the papers in Table 7.2 displayed a visual representation or had a dimension that represented the physical vaporiser, therefore these models would be classified as 0-D.

2.5.3.2 Model Summary

From the papers found, using Black Box models, the papers produced since 2018 were further analysed. A summary of the models developed in those papers follows: this is used to summarise common practices and results of Black Box models.

Palagi et al., 2019 employed three different methods in Python, namely Feed Forward Neural Networks (FF), Recurrent Neural Networks (RNN) and Long Short-Term Memory Neural Networks (LSTM). These were used in modelling a waste heat ORC Cycle utilising a thermal oil interface circuit. This unit had a gross power generation of 20 kW. All the aforementioned methods showed a percentage error lower than 10% in predictions 60 seconds ahead and lower than 5% in predictions 10 seconds ahead. Of these methods, the best performing was the LSTM-NN with a Root Mean Square Error (RMSE) of 0.03 to 0.08 in the predictions of mass flow rate, pressure and turbine inlet of the working fluid.

Mert et al., 2020 compared step-wise Multi-Linear Regression models (MLR), a FF-NN with varying structures and a hybrid MLR and FF model. These models were employed in predicting the generated power of the turbine of a 10 kW waste heat ORC system. Of these methods, the hybrid MLR-NN model performed the best with an RMSE of 0.047–0.20.

Peng et al., 2021 developed a steady state model to be used in the prediction of heat transfer across the vaporiser. A Back Propagation NN was used to produce this model. For the heat transfer predictions across the vaporiser, an R^2 of 0.9999 for both validation and test sets was achieved. The average absolute deviation (AAD) for this prediction was 0.56%. Other variables such as net work of the system and thermal efficiency were also predicted, which displayed similar errors. This data was generated and validated against REFPROP.

Kovacı et al., 2017 compared FF-NN and an Adaptive Neural Fuzzy Inference System (ANFIS) in steady state modelling of a WHR ORC system. The R^2 value of the FF-NN and ANFIS were 0.99 and 0.97, respectively, for the R-365mfc working fluid. The primary purpose of these models was to be further used in the design of ORC systems.

Kılıç and Arabacı, 2019 developed a BP NN and ANFIS model based on generated data using CoolPack which is a collection of simulation models for refrigeration systems. In this study, various working fluids were tested for prediction of the thermal efficiency using the BP-NN and ANFIS. For the working fluid R123, an R^2 and an RMSE value of 0.999 and 0.02 and 0.996 and 0.0056 was achieved, respectively.

Comparison of a Support Vector Machine (with both a radial based kernel function and a linear function) model against a BP-NN was carried out by Dong et al., 2018. These models were used in the prediction of the output work of the system. The best performance was shown with SVM linear function and BP-NN. The SVM linear function model achieved an R^2 and RMSE of 0.998 and 0.41, respectively and the BP-NN achieved 0.998 and 0.30, respectively. This was found when 40% of the available data was used for testing.

Yang et al., 2018 produced a BP-NN used in dynamic predictions of the power generated from the turbine of a lab-sized ORC system. This system had a gross power of 4.8 kW and was used in waste heat recovery, data from which was used to generate and validate the NN. A genetic algorithm was used to optimise the weights of the NN. The absolute prediction error for this model ranged up to 0.2 kW. This model was utilised for operational improvements to the system.

Khosravi et al., 2019 modelled a geothermal and solar system, where the solar unit was used in superheating the working fluid. A Multi-Layer Perceptron (MLP) NN and ANFIS were used with particle swarm optimisation to update the model parameters. The R^2 and RMSE for the validation of the ANFIS model were 0.999

and $3.587e^{-4}$, respectively, for predicting the energy efficiency of the system while the MLP-NN achieved an R^2 and RMSE of 0.9954 and $7.574e^{-4}$, respectively. The exergy efficiency and net work were also predicted, with similar prediction errors shown. The model was produced for the design of a novel system and for assessing its economic feasibility.

A dynamic NN model was produced of a geothermal power plant by Liu et al., 2021. Although a generation capacity was not specified, however, this particular plant is operated by Cyrq Energy Inc. This model was trained, validated and tested on different data sets from the industrial plant data. An R^2 of 0.97 was achieved for both the working fluid outlet and brine outlet of the vaporiser.

Wang et al., 2020 produced a BP-NN and a Support Vector Regression (SVR) model for the prediction of thermal and exergy efficiency for various working fluids. The Mean Relative Error (MRE) of the BP-NN and SVR models maintained values of about 1%- 5% and 1% - 2% respectively, for the thermal energy efficiency. These previous values describe results from the basic ORC system with various working fluids, however other system configurations are also used in predictions with comparable results. These models were developed in Python and based on and validated against data generated from REFPROP. The main purpose of these models was to compare modelling methods for design. The type of system modelled was a waste heat system.

Yan et al., 2021 compared a MLR, SVR and BP-NN steady state model in MATLAB. This was used in the prediction of thermal efficiency and net power output. The system utilised waste heat and a thermal interface oil loop and had a capacity to generate 10 kW. Data from this system was used to validate and test the model. All models achieved R^2 values greater than 0.995 for net power output and greater than 0.977 for thermal efficiency. The SVR model showed the highest accuracy. All models showed similar findings with a lower RMSE than 0.055, where the SVR model performed the best.

Enayatollahi, Fussey, and Nguyen, 2020 developed a dynamic model of a 1 kW ORC waste heat cycle, which was based on data from this lab-scale unit. The gradient descent-based approach and Particle Swarm Optimisation (PSO) were used in training the ANFIS model. An R^2 of 0.98 and 0.99 for predicting the outlet temperature of the brazed plate vaporiser were obtained for the gradient descent approach and PSO learning methods, respectively. These results also showed an RMSE of

3.4°C and 2.4°C, respectively.

A dynamic fuzzy-based model was produced of a 4.5 kW ORC WHR system by Chowdhury et al., 2018. This model was based on and validated against data generated from a FP discretised model. The results showed a RMSE error of 1.1K and 3.1K for the outlet temperature of the refrigerant and heat source, respectively.

Huster, Schweidtmann, and Mitsos, 2019 used data generated from CoolProp in predictions of the thermodynamic properties for optimisation of design conditions of the ORC system. A NN model was used which was developed in MATLAB. This work was extended by Huster, Schweidtmann, and Mitsos, 2020, where a model was used in the thermoeconomic optimisation of a geothermal ORC unit. Schweidtmann et al., 2019 then developed a steady state model based on a validated dynamic model of a waste heat unit by Huster et al., 2018.

Zhi et al., 2019 produced a steady state model for the design of an ORC waste heat system. A BP-NN was based on data generated from REFPROP in MATLAB. This model was validated against another study (Cayer et al., 2009), and was used in the prediction of the thermal efficiency and exergy efficiency of the ORC system with and without a recuperator. The results show an RMSE and AAD of 0.044 and 0.52% respectively.

Feng et al., 2020 developed a BP-NN for predicting the net power output and thermal efficiency of a 3 kW experimental ORC waste heat system. Experimental data from this system was used in the training and validation of the model. The absolute error of the thermal efficiency predicted by the model is in the range of $10 \times 10^{-4} - 6 \times 10^{-4}$, and the absolute error of the net output work is 0.03 – 0.04 kW.

2.6 Comparing First Principles and Black Box Models

First Principles (FP) models take more time to create, tune and validate when compared with Black Box models. However, this comes with the added benefit of the robustness of FP models. As Black Box models are generally valid only at the tested conditions, the as-built model will therefore struggle in the simulation of extreme conditions. This limits the application of Black Box models. FP models are able to more accurately simulate extreme conditions and may be applied to new vaporiser models as a result of the theoretical modelling approach (Quaak, Wijck, and Haren, 1994; Rasmussen, 2012).

Black Box models are also highly dependent on the data set. Practically, Black Box models can be used only when sufficient inputs and outputs are measured, which may prevent some applications in industrial settings (Yin et al., 2014; Quaak, Wijck, and Haren, 1994). Black Box models work well in situations where the mechanisms are not completely understood or simplification of a model is required. This is where white box models struggle. Deriving unknown or complex relationships of a FP model from data has been shown to work well in improving model efficiency. In some cases, it was shown that Black Box models outperformed FP models in model accuracy (Russell, 1997). Incorporating aspects of both of these models has been termed 'grey box' or 'hybrid modelling'.

2.7 Grey Box Models

As stated in Section 2.6, Grey Box models incorporate aspects of both FP and Black Box models. Grey Box models are developed through integrating sub-models of different types. This can be implemented through various structures such as in series, in parallel or surrogate modelling (Sansana et al., 2021).

The only model of ORCs classified as a Grey Box model is (Kalina and Świerzewski, 2019). In this model, an industrial, biomass-fired co-generation plant was simulated. This system had a net power generation of 1300 kW. A dynamic model was developed, capable of predicting the heat duty of the vaporiser. The predictions were validated against plant data, showing an R^2 of 0.98 and a RMSE of 260 kW. The model was capable of other predictions, showing similar accuracy to the aforementioned prediction.

2.8 Conclusions

As described in this chapter, a large number of papers has been published based on theoretical and experimental performance of small scale ORC systems (Kalina and Świerzewski, 2019). A majority of models produced in the literature focus on FP models, however, these models have key advantages over Black Box models, namely, their robust nature allows predictions over a wide range of conditions. As the mechanisms for heat transfer are well-understood, FP models can be seen as more suitable for modelling vaporisers.

Of the FP models found in the literature, six models were validated against data from large-scale, industrial processes (Altun and Kilic, 2020; Pili, Spliethoff, and Wieland, 2017; Proctor et al., 2016; Mazzi, Rech, and Lazzaretto, 2015; Sun and Li, 2011; Sohel et al., 2010). These predominantly were dynamic models with the model purpose of control strategy testing and operational optimisation and design. Of these models, four have been produced based on geothermal applications, covering various modelling methodologies. These include lumped models produced by (Proctor et al., 2016; Sohel et al., 2010) and the two-volume model by (Pili, Spliethoff, and Wieland, 2017).

Of the dynamic models found in the literature, Aspen HYSYS has yet to be applied to a geothermal industrial application, in addition no First Principles model was developed using Python. Of the First Principles models described, each spatial paradigm and heat transfer paradigm has benefits that can suit a specific modelling purpose. Due to the discretised method's flexibility to scale the number of discretised sections, and the relative simplicity of the equations needed, the discretised methodology was selected. The temperature difference method was selected for the heat transfer paradigm, as this is most suitable for dynamic applications.

To address the gap in comparative analysis of large-scale geothermal models and to add to the small group of dynamic models, this thesis will focus on developing, then comparing, modelling techniques of the Ngawha geothermal power plant's vaporiser. The models will be developed in Aspen HYSYS and Python to ascertain if these software tools can effectively model a geothermal application.

Chapter 3 will describe details of the system itself.

Chapter 3

Case Study

3.1 Preface

Chapter 3 covers the background of the system modelled in this thesis, the Ngawha OEC4 Geothermal binary plant operated by Top Energy. This work focuses on the working fluid cycle of the plant and validates the models developed with two snapshots of the plant's human-machine interface (HMI). An explanation will also be given of the production delivery system and details of the plant's background.

3.2 System Description

The Ngawha OEC4 Geothermal binary plant is located north of the Ngawha Springs area alongside three other geothermal plants. The Ngawha plant can generate a gross 35 MW during normal operation. The geothermal brine and steam are separated by OEC4's own separator plant. A dual turbine system is used, in addition to air-cooled condensers. The system uses normal pentane as the working fluid, which passes through several pre-heaters in order to extract heat from the brine and the condensed vapour. Additionally, a non-condensable gas (NCG) pre-heater is used to heat the working fluid bypass. Recuperators are also used in recovering heat from the turbine outlets. The plant SCADA data readings are shown in Table 3.1. Operational data of the working fluid cycle was not received due to contractual confidentiality. Discussion on approximating the turbine efficiency and the working fluid flow-rate is shown in Section 4.2.5.

TABLE 3.1: Table describing the plant readings. The working fluid flow-rate and turbine efficiency are approximated

Plant Specification	Value	Units
Working Fluid Flow-rate	1343.6	tonne/h
Working Fluid Pressure	26.18	bar
Working Fluid Temperature	61.6	°C
Brine Flow-rate	1199	tonne/h
Brine Pressure	14.51	bar
Brine Temperature	191.1	°C
Steam Flow-rate	105	tonne/h
Steam Pressure	12.76	bar
Steam Temperature	189.7	°C
Expander Efficiency (Isentropic)	85	%
Ambient Air Pressure	1.013	bar
Ambient Air Temperature	17.1	°C

3.3 Production Delivery System

In liquid-dominated regions such as those used by binary systems, the geothermal fluid flows naturally from the reservoir to the surface. The pressure of the fluid is reduced, therefore vapour flashes in the well, resulting in a two-phase mixture. The system involved in the transportation of this geothermal mixture is the production delivery system, whereby this mixture is separated into vapour and liquid phases. These fluids are then used in vaporising and pre-heating the working fluid. This differs from flash steam plants in that flashing of the two-phase mixture produces vapour, which is then used to drive the turbine.

3.4 Plant Description

As described in Section 3.3, the two-phase geothermal fluid is fed into a separator. In this separator, the two phases are split into vapour and liquid streams, each of which passes through a vaporiser. Following the outlet of the vapour side, this fluid is partially condensed and then enters the vaporiser separator. The condensate is

reincorporated with the brine, while the remaining vapour enters the tubes of the non-condensable gas pre-heater.

The two-phase fluid, including the condensate and remaining gaseous steam and non-condensables, is separated. The vapour is vented to the atmosphere while the condensate is incorporated into another portion of the brine stream. The brine entering the vaporiser tubes makes two passes, then passes through three pre-heaters in series. After reincorporating the brine with both condensate streams, it is sent to the reinjection system. The working fluid passes through the shell-side of these three heat exchangers. A bypass is made for the working fluid around these heat exchangers which passes through the shell-side of the NCG pre-heater. This is used in optimising the temperature of the working fluid entering the vaporiser. The working fluid exiting the vaporiser enters two identical turbines and then the shell-side of two identical recuperators. For simplicity, one recuperator and turbine are shown in Figure 3.1. After exiting the recuperator, the working fluid is condensed in an air-cooled condensor. The fully liquid working fluid is pressurised and enters the tube-side of the recuperators, and on exiting these recuperators, the cycle is complete.

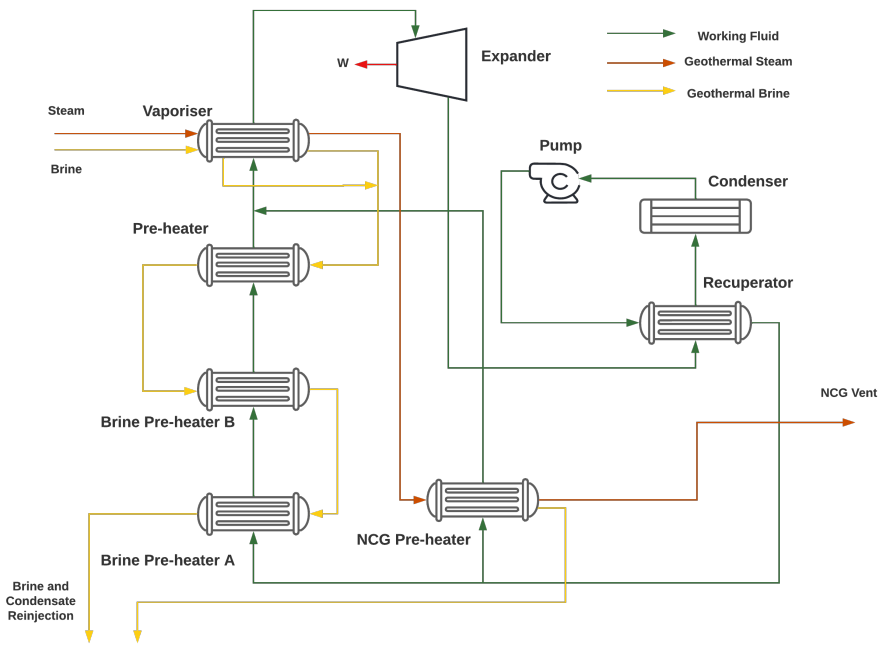

FIGURE 3.1: A simplified process flow diagram of the working fluid cycle of the Ngawha OEC4 plant

3.4.1 Vaporiser Configuration

As described in Section 3.4, the vaporiser has multiple tube-sets, for brine and for geothermal vapour. The basic configuration is shown in Figure 3.2. The brine tubes have two passes, which carry out the sub-heating and a small amount of vaporisation of the working fluid, while the geothermal vapour carries out the remainder of the vaporisation and a degree of superheating of the working fluid in a single pass. The working fluid flows perpendicular to the flow of the geothermal fluids.

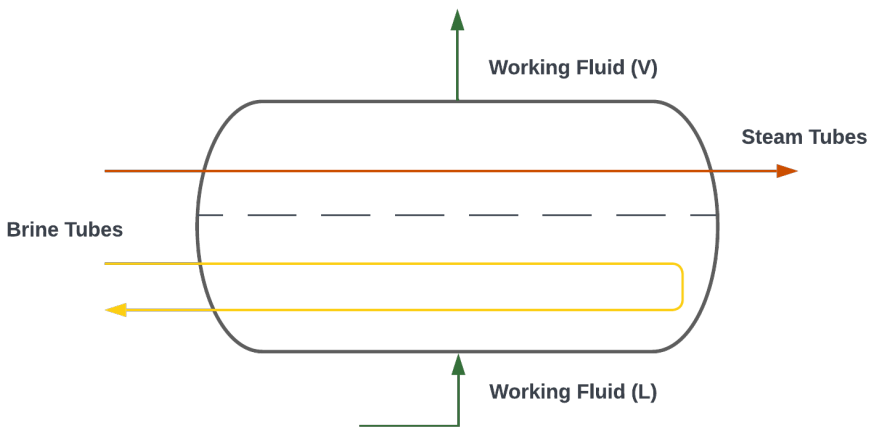

FIGURE 3.2: The vaporiser shell and tube configuration for Ngawha OEC4 plant

3.5 Geothermal Fluid Composition

Geothermal fluid is formed through the natural movement of water through the Earth's crust. As such, the composition of a geothermal fluid consists of a complex mixture of water, salts and gases (DiPippo, 2016; Talybov, Azizova, and Abdulagatov, 2019). This composition varies with each region, depth and type of geothermal reservoir. This is explained in more detail in DiPippo, 2016.

The composition of a geothermal vapour is strongly related to its thermodynamic properties and therefore requires a 'fit for purpose' equation of state in order to be modelled most effectively. With access to the geothermal plant's compositional analysis, the vapour is largely comprised of water and a small amount of carbon dioxide. Minuscule amounts of Methane, Ammonia, Hydrogen Sulfide, Hydrogen and Nitrogen were also shown by this analysis, however, the mole fraction was less than

0.0001 and was therefore deemed unnecessary. The brine is assumed to be pure water as the changes to the thermodynamic properties of the fluid are relatively small when compared with vapour. The simplified mole fraction of the separated vapour used in the following models is shown in Table 3.2.

TABLE 3.2: The composition of simplified geothermal vapour

Component	Mole Fraction
Water	0.985
Carbon Dioxide	0.015

3.6 Conclusions

This chapter provides an overview of the system that is modelled in this work. A simplified process flow diagram and a diagram representing the vaporiser configuration is shown in Figures 3.1 and 3.2, respectively. Plant readings and the simplified composition of geothermal vapour are shown in Tables 3.1 and 3.2, respectively. These are used as inputs to the models developed in Chapter 4.

Chapter 4

Vaporiser and Plant Modelling

4.1 Preface

Chapter 4 covers the development of the plant model and the vaporiser models. These include a vaporiser and plant model developed in Aspen HYSYS and a vaporiser model developed in Python. All models were developed and tuned against snapshots of plant conditions at steady state. The vaporiser models were transitioned into dynamics where a dynamic response was compared. This comparison is made between a widely used, commercial process simulator and a First Principles model developed in this thesis.

4.2 Aspen HYSYS Model

Aspen HYSYS is widely used in both industry and academia in analysing process engineering applications in steady state and dynamics. This software package has yet to be applied to analyse a dynamic model of an industrial-scale geothermal binary plant and vaporiser. As such, Aspen HYSYS was selected in the development of a dynamic model of the vaporiser. In addition to this, a plant model of the working fluid cycle was developed in steady state. A flow diagram of this model is shown in Figure 4.1.

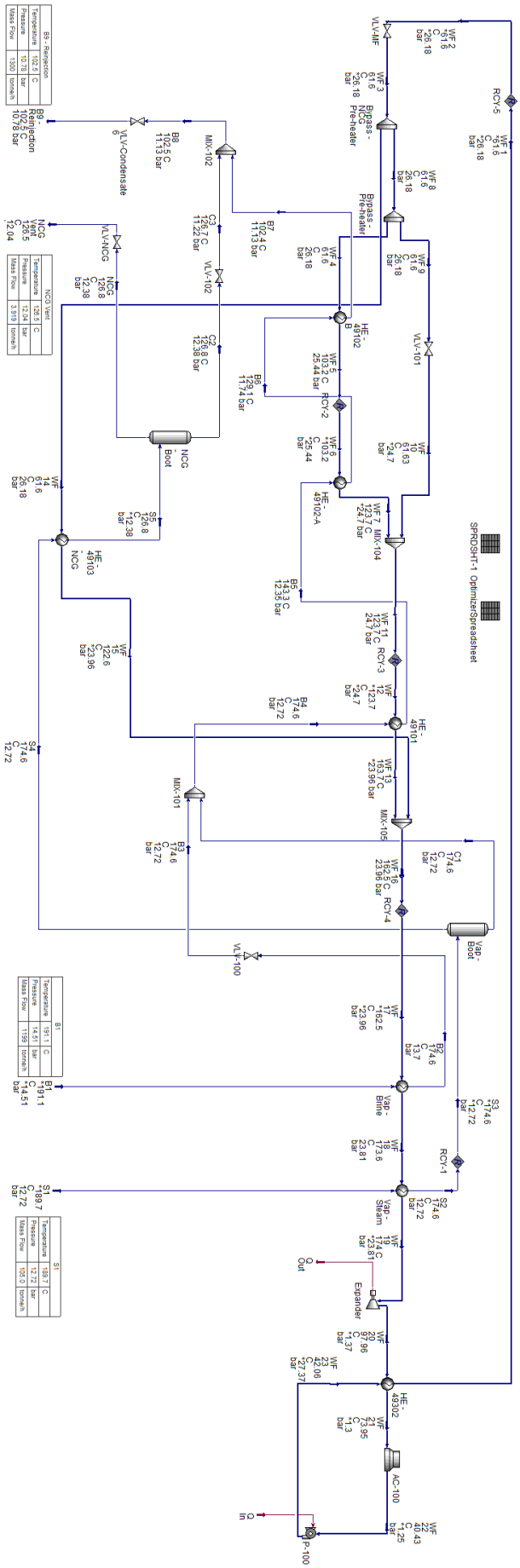

FIGURE 4.1: Aspen HYSYS schematic of plant and vaporiser model. Specified stream conditions are noted in tables.

4.2.1 Modelling Procedure

There is no unit operation provided by Aspen HYSYS that replicates a multiple tube-set heat exchanger. The approach taken is based on the method developed by Proctor et al., 2016, where two coolers were used to model the heat transfer of each tube-set in addition to a heater modelling the heating of the shell side. The LMTD was calculated for each section and these were multiplied by the static UA values calculated based on plant data. The resultant heat flow was summed and used for specifying the shell-side heater. This approach worked well, however a limitation identified was the static UA values. As a result, a different approach was taken for the heat transfer coefficients of this model. To facilitate this, two heat exchangers are used in contrast to the two coolers and heater used by Proctor et al., 2016. The Aspen HYSYS schematic is shown in Figure 4.2.

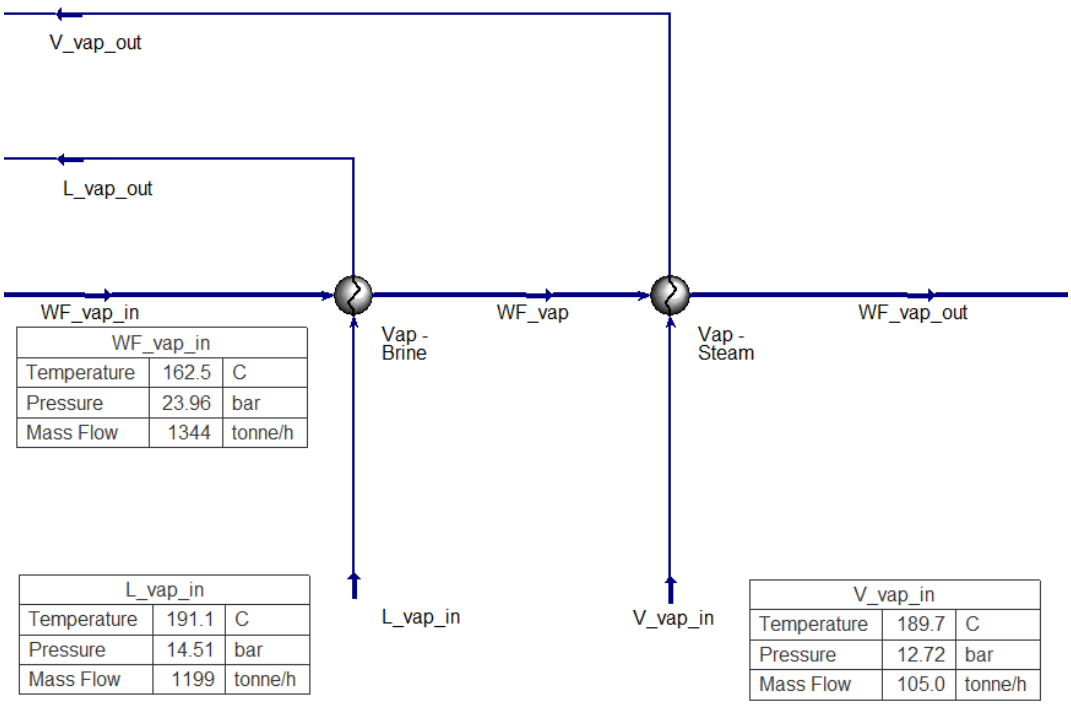

FIGURE 4.2: The Aspen HYSYS schematic of the vaporiser model. The Vap - Brine and Vap - Steam refer to the brine and geothermal steam of the vaporiser.

4.2.2 Heat Transfer Coefficients

In approximating the heat transfer coefficient (HTC), empirical calculations were used to predict temperature differences over a range of conditions.

A nucleate boiling correlation was selected for the vaporising of the working fluid due to the mechanisms of the kettle re-boiler, whereby a pool of working fluid accumulates bubbles which nucleate on the outer tube-side wall. Researchers such as Pili, Spliethoff, and Wieland, 2017, have tested the Mostinski correlation in a kettle re-boiler with butane as the working fluid. This was compared with the Cooper equation (Cooper, 1984). Similar comparisons have also been made by Calise et al., 2018, however, contradictory results suggest that the ideal heat transfer coefficient may be system-specific. Due to its relative simplicity, the Cooper equation was chosen, Equation 4.1.

$$U = Constt55P_r^{0.12-0.2log_{10}R_p} log_{10}P_r^{-0.55} M_w^{-0.5} Q_{flux}^{0.67} \tag{4.1}$$

Where $Constt$ is equal to 1.7 as this contacts a cylindrical surface, P_r is the reduced pressure, R_p is the surface roughness of the pipe, M_w is the molecular weight of pentane $72.15gmol^{-1}$, Q_{flux} is the heat flux in Wm^{-2}.

In the pre-heating of the working fluid, the convective coefficient for the working fluid is classified as flow perpendicular to banks of tubes (Carta, 2021; McAdams, 1954). The HTC was found from Equation 4.2.

$$Nu = bRe^n Pr^{1/3} \tag{4.2}$$

Where b and n values were used from Grimison, 1937. These values correspond to the pitch and diameter of the tube bundle.

The heat transfer coefficient between carbon dioxide and condensing steam mixture and the wall is shown in Equation 4.3. This has been described as an annular two-phase flow regime whereby the condensed water accumulates on the wall surface while the vapour flows in the centre of the pipe (Sinnott, 2005). Researchers such as (Siwach, 2016) have used the correlation proposed by (Dobson and Chato, 1998). Other correlations such as Cavallini et al., 2006; Shah, 1979 have been suggested by Dobson and Chato, 1998. These correlations were compared, however, the correlation proposed by (Dobson and Chato, 1998) showed better performance. This was used in both the steam section of the vaporiser and the NCG pre-heater.

$$Nu = 0.023Re_L^{0.8} Pr^{0.4} \left[1 + \frac{2.22}{X_{tt}^{0.89}}\right] \tag{4.3}$$

Where the Re_L is the Reynolds number of the liquid and the Lockhart-Martinelli parameter $X_{tt}$is defined as follows:

$$X_{tt} = \frac{1-x}{x^{0.9}}(\rho_v/\rho_l)^{0.5}(\mu_l/\mu_v)^{0.1} \tag{4.4}$$

Where x is the vapour fraction leaving the steam tubes, ρ_v and ρ_l are the density of the vapour and liquid and μ_v and μ_l are the viscosity of the vapour and liquid.

In approximating the convective coefficient for the geothermal brine and condensate, the Haaland equation was used for the friction factor (Haaland, 1983). Gnielinski's equation (Gnielinski, 1975) (Equation 4.5) was then used in approximating the Nusselt number for turbulent flow in a pipe. A relative roughness of the pipe was assumed, based on Kandlikar, Joshi, and Tian, 2003; Wu and Little, 1984.

$$Nu = \frac{(f/8)(Re-1000)Pr}{(1+12.7(f/8)^{1/2}(Pr^{2/3}-1)} \tag{4.5}$$

Where f is the Haaland friction factor calculated from:

$$\frac{1}{\sqrt{f}} = -1.8log\left[\frac{\epsilon/D}{3.7}^{1.11} + \frac{6.9}{Re}\right] \tag{4.6}$$

4.2.3 Equations of State

Careful consideration must be taken in selecting the Equations of State (EOS) as this is necessary for an accurate model as it handles the calculation of state variables under given conditions. Based on Peng-Robinson's wide use in the modelling of hydrocarbons, it was selected for use with the pentane working fluid (Aspen Technology, 2013). Aspen HYSYS' Peng Robinson package was also compared with data available from the National Institute of Standards and Technology (NIST) by Haydary, 2019, where agreeable results were shown. The Peng Robinson EOS used in Aspen HYSYS uses enhanced binary interaction parameters, therefore differs slightly from the standard Peng Robinson EOS (Haydary, 2019).

Modelling a vapour mixture of water and carbon dioxide can be difficult due to the complex interactions between the polar water and non-polar carbon dioxide molecule. Extensive research into mixtures of higher mass fraction carbon dioxide has been conducted, however, this range is outside the carbon dioxide mass fraction seen in geothermal applications (Talybov, Azizova, and Abdulagatov, 2019;

Colucci et al., 2019). From the literature, various suggestions have been made for cubic-based equations of state including Peng-Robinson, Redlich-Kwong and Cubic-Plus-Association equations (Talybov, Azizova, and Abdulagatov, 2019; Colucci et al., 2019). Other EOS, such as multi-parameter Helmholtz-based equations used in REFPROP and CoolProp (Lemmon, Huber, and McLinden, 2013; Bell et al., 2014) which are not available in Aspen HYSYS, will be discussed in later sections. Of the suggestions that are available through Aspen HYSYS, the Peng Robinson (PR), Peng Robinson Twu (PR-Twu), Peng Robinson Stryjek Vera (PR-SV) and Cubic-Plus-Association (CPA) EOS were tested in calculating the saturation pressure at a temperature specified by plant conditions. PR and Soave Redlich-Kwong (SRK) Sour were also tested as these were considered potential options. Modelling of the NCG vent mass flow-rate was tested with the aforementioned EOS. This was done by replicating the geothermal vapour and NCG flows through the plant whereby the vapour passes through the vaporiser and is separated. The separated vapour then passes through the NCG pre-heater and is separated again. The resultant vapour, largely made up of NCG, is vented. The NCG mass flow-rate predictions are shown in Table 4.1.

TABLE 4.1: Comparison of Equations of State in calculating the saturation pressure and NCG mass flow-rate of the plant model

EOS	Sat. Pressure (bar)	Error (%)	NCG Mass Flow (T/h)	Error (%)
CPA	12.72	0.31%	3.66	30.29
PR Twu	12.62	1.10%	3.65	30.5
PR SV	12.66	0.78%	3.68	29.9
PR Sour	12.65	0.86%	3.58	31.8
SRK Sour	12.65	0.86%	3.58	31.8
Measured	12.76		5.25	

The percentage error was calculated using the Equation 4.7.

$$\%Error = \frac{y_{meas} - y_{pred}}{y_{meas}} \times 100\% \tag{4.7}$$

From these results, the Cubic-Plus Association EOS shows the lowest error at 0.31%, followed by the PR-SV EOS at 0.78%. The CPA and PR-SV perform the best for the NCG mass flow-rate test at 30.29% and 29.9% percentage error, respectively, although none of the tested EOS performed adequately. Based on these basic results,

the EOS does not capture the chemical interactions of the mixture effectively, however further research is required for a more conclusive result.

4.2.4 Model Specifications

In the development of an Aspen HYSYS model, key stream characteristics and equipment can be specified. The geometry of the pre-heaters was approximated based on ratios of the vaporiser geometry. These values were then used, in addition to fluid conditions, to calculate the empirical HTC described previously, for each heat exchanger in the system. In each heat exchanger a pressure drop was specified on both shell and tube streams. An isentropic efficiency of 85% was assumed for the turbine, and pressure specifications were also made on the outlet to the turbine as this value remained relatively constant. Similarly, the working fluid pressure and temperature were specified leaving the recuperator. The mass flow-rate at this point and the bypass flow-rate is also specified. However, further details in the method of approximating these mass flows are shown in Section 4.2.5. The compositions, the mass flow-rate and the temperature were specified for both geothermal fluids. However, saturated conditions were assumed for the geothermal vapour. The brine pressure was also specified. The aforementioned specifications are displayed in Table 3.1.

4.2.5 Approximating Working Fluid Flow-rate

Due to the nature of a binary geothermal plant there are no readings of working fluid flow-rate as this is controlled by adding and removing from a working fluid storage system. This flow-rate dictates key temperature differences across all heat exchangers in the working fluid cycle of the plant, therefore an approximation needs to be made of not only the main flow-rate but also the bypass flow. An optimisation was conducted using Aspen HYSYS's inbuilt optimiser. The first optimisation was based on the working fluid bypass through the NCG bypass, where a minimum absolute difference between the model and the plant reading of the working fluid temperature was found. The second optimisation was conducted in a similar manner to the first, although this was based on the working fluid inlet flow to the vaporiser. The optimised flows are shown in Table 4.2.

These results were then supported by comparing the power generated by the turbine in the model to a plant specified value. An error of less than 1 MW in

both cases shows agreeable results for this optimisation. The resultant discrepancy against plant data is shown in the following Tables 4.3 and 4.4.

TABLE 4.2: Optimised working fluid mass flow-rate for Case 1 and 2

Approximated Mass Flow-rate	Case 1	Case 2
$\dot{m}_{wf_T}$ (T/h)	1343.6	1220.0
$\dot{m}_{wf_ncg}$ (T/h)	45.1	19.1

4.2.6 Model Tuning

To match the outlet temperatures to the plant's equipment, the HTC was multiplied by a tuning factor. The tuning factor matches the HTC to the specific exchangers' geometries. This has the proposed benefit of replicating the behaviour of the system over a range of plant conditions. The model was tuned to the steady state data from the plant, shown in Table 4.3. The condensate reinjection and NCG pre-heater showed the largest discrepancies of the model with an absolute error of $6.77°C$ and $5.52°C$, respectively. This discrepancy is discussed below in Section 4.2.7.

TABLE 4.3: Steady state results of plant and vaporiser of Case 1

Fluid Variable	Plant Data	Hysys Model	Error Abs.	Error (%)
$T_{wf_vap_out}$ (°C)	174.00	174.03	0.03	0.02
$T_{v_vap_out}$ (°C)	174.80	174.63	0.17	0.10
$T_{l_vap_out}$ (°C)	174.60	174.55	0.05	0.03
$T_{wf_vap_in}$ (°C)	162.50	162.48	0.02	0.01
$T_{v_ncg_out}$ (°C)	120.00	126.77	6.77	5.64
$T_{l_inj_out}$ (°C)	97.00	102.52	5.52	5.69
P_{gen} (MW)	34.94	35.14	0.20	0.58

4.2.7 Steady State Model Validation

The second case against which the model was validated, showed significantly different plant conditions from Case 1. This was due to the change in ambient temperature and therefore differing optimal conditions of the plant, as deemed by the operator. These results show good agreement for all streams leaving the vaporiser, with less than a degree error, which is less than the expected error of the temperature sensors. However, an even larger error is shown in the outlet NCG temperature of the NCG pre-heater. A significant discrepancy is also shown in the percentage error of this stream's mass flow-rate. To support the model's prediction, a mass balance of CO_2

was done. This showed approximately 95% of the CO_2 leaving the system through this stream, with the remaining leaving the system in an aqueous solution as a result of the separation processes. This is thought to be a limitation of the EOS in state calculations of the carbon dioxide and water mixture. The flow-rate of this stream is comparatively small relative to the working fluid and condensate flow-rates at 3.92T/h and 3.61T/h in Case 1 and Case 2 respectively. Another notable error is shown on the condensate reinjection stream, with an absolute error of 5.52°C and 2.91°C in Case 1 and Case 2 respectively. This is thought to result from the approximations of geometrical data of the pre-heaters, thus could be remedied through the implementation of this geometrical information.

TABLE 4.4: Steady state results of plant and vaporiser of Case 2

Fluid Variable	Plant Data	Hysys Model	Error Abs.	Error (%)
$T_{wf_vap_out}$ (°C)	170.10	170.17	0.07	0.04
$T_{v_vap_out}$ (°C)	170.40	170.30	0.10	0.06
$T_{l_vap_out}$ (°C)	170.80	170.83	0.03	0.02
$T_{wf_vap_in}$ (°C)	156.70	157.71	1.01	0.64
$T_{v_ncg_out}$ (°C)	105.00	135.39	30.39	28.94
$T_{l_inj_out}$ (°C)	95.90	92.99	2.91	3.04
P_{gen} (MW)	31.96	31.28	0.68	2.13

4.3 First Principles Model

Based on the four approaches described in Chapter 2, the discretised modelling method was selected. This is based on its higher accuracy than the corresponding moving boundary and lumped methods. This method also has the added flexibility in the level of discretisation such that the model parameters can be changed to reflect its purpose (Huster et al., 2018). A discretisation of 20 was selected as this was shown by literature, along with heuristics, to have a good balance between processing speed and accuracy.

4.3.1 Software

The model was developed in Python using solve_ivp integrator from SciPy integrate, where the explicit Runge-Kutta method of order 3(2) was used in solving the ODE. The model utilised Coolprop for the thermodynamic package. Python and CoolProp were used as they are widely available, with both being open source and free programs.

4.3.2 Model Formulation

The governing equations of the vaporiser are the working fluid mass and energy balance, the geothermal fluid mass and energy balance, and the energy balance of the wall. First, the following assumptions were made for simplification of the differential equations solution:

- No axial heat conduction, only heat transport, in the working fluid, wall or geothermal fluid.
- Spatially constant fluid pressure p(t).
- The three tube passes are each discretised into a number (n) of lumped sub-volumes, each of which corresponds to a sub-volume of the shell.
- The geothermal fluid and working fluid temperature profile of each section are static.
- Inlet and outlet enthalpy are averaged in order to approximate the temperature of the section.
- The mass flow-rate for each individual fluid is equal in all sections.

- The geothermal vapour composition is assumed to contain CO_2 and water. The mole fraction is specified in Table 3.2.

The resultant differential equations are shown below.

Working fluid mass balance:

$$\frac{\partial(A_{wf}\rho_{wf})}{\partial t} + \frac{\partial \dot{m}_{wf}}{\partial z} = 0 \tag{4.8}$$

The working fluid energy balance:

$$A_{wf}\rho_{wf}\frac{\partial h_{wf}(z,t)}{\partial t} = -\dot{m}_{wf}\frac{\partial h_{wf}}{\partial z} + \pi d_o U_{wf}(T_w - T_{wf}) \tag{4.9}$$

The geothermal fluid mass balance:

$$\frac{\partial(A_{gf}\rho_{gf})}{\partial t} + \frac{\partial \dot{m}_{gf}}{\partial z} = 0 \tag{4.10}$$

The geothermal fluid energy balance:

$$A_{gf}\rho_{gf}\frac{\partial h_{gf}(z,t)}{\partial t} = \dot{m}_{gf}\frac{\partial h_{gf}}{\partial z} + \pi d_o U_{gf}(T_w - T_{gf}) \tag{4.11}$$

The wall energy balance:

$$\rho_w Cp_w A_w L\frac{dT_w(z,t)}{\partial t} = N_t \pi d_i U_{gf}(T_w - T_{gf}) + N_t \pi d_o U_{wf}(T_w - T_{wf}) \tag{4.12}$$

4.3.3 Cross-flow Configuration

In developing this model, the working fluid was segmented into three vertical sections. These corresponded to the three passes of geothermal fluid through the vaporiser. Section 1 corresponded to the brine tube-set second pass, Section 2 corresponded to the brine tube-set first pass and Section 3 corresponded to the steam tube-set. To solve Section 1, the temperature of the brine leaving Section 1 is needed. Both sections are then solved using a loop until the brine outlet enthalpy of Section 2 matches the brine inlet enthalpy of Section 1. This was done with a relative tolerance of 1 e^{-5}. A diagram describing this configuration is shown below in Figure 4.3.

4.3.4 Heat Transfer Coefficients

The Haaland equation was used for friction factor and Gnielinski's HTC were used for brine tubes (Haaland, 1983). The Dobson equation was used for the HTC of

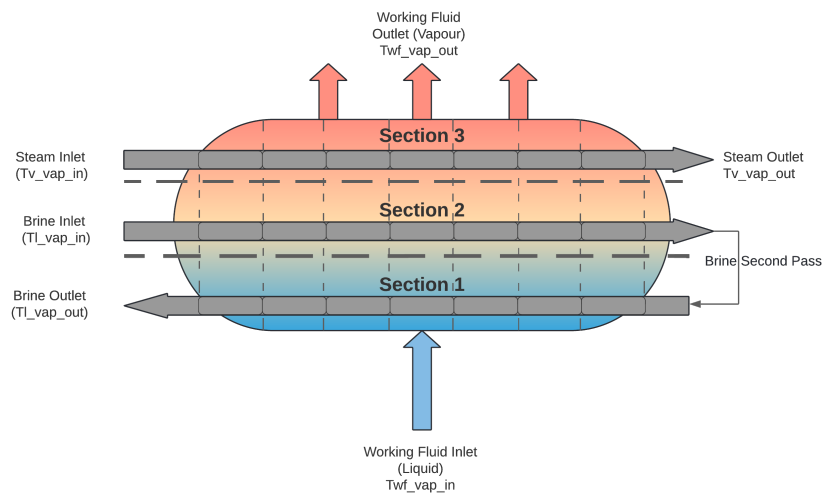

FIGURE 4.3: Configuration of the First Principles model with a discretisation of seven

condensing geothermal vapour and the Cooper correlation was used for the nucleate boiling HTC of the working fluid (Cooper, 1984; Dobson and Chato, 1998). In the previous Section 4.2.2, the heat transfer coefficients decisions were described in more detail.

4.3.5 Equations of State

Much like section 4.2.3, Peng Robinson was used for the working fluid. However, differing from Aspen HYSYS, CoolProp uses the multi-parameter Helmholtz EOS. This EOS was the most suitable of the three available in CoolProp. The approach taken by CoolProp in characterising the behaviour of carbon dioxide and water mixtures utilises empirical mixing terms to improve its thermodynamic description (Harvey et al., 2016; Lemmon, Huber, and McLinden, 2013; Bell et al., 2014).

4.3.6 Data-Driven Correlations

Based on the approach taken by (Huster, Schweidtmann, and Mitsos, 2020), thermodynamic data generated from CoolProp was used in developing empirical correlations for temperature and density. These correlations were developed as an alternative to using CoolProp while running the simulation, which led to slow processing speeds. Comparatively, in Huster, Schweidtmann, and Mitsos, 2020 the models produced are simpler. The curve fit function from SciPy for fitting power functions and

Polyfit from NumPy for linear and polynomial functions were used. Though this approach is simpler, the range of conditions for which these models are valid is small. Consequently, adequate results are shown in Table 4.5.

4.3.6.1 Temperature and Density Curves

The equations shown in the formulation of these models are in terms of enthalpy. In calculating the heat transfer the temperature must be known, therefore a relationship was derived. These models were extended to incorporate pressure in order to adapt to changing pressure conditions of the plant. One standard deviation above and below the mean from plant data was selected for temperature and pressure ranges for the geothermal fluids. Approximately 10,000 data points were generated for each curve. Each curve fitted follows a similar method, fitting the temperature in terms of enthalpy at the specified range of pressures. The change in the various coefficients is then fitted in terms of pressure using Polyfit.

In order to effectively model the phase change of the normal pentane working fluid, over a range of temperatures, a piece-wise modelling approach was taken. A relationship predicting density was also fitted in the same piece-wise form. This required a dew curve, a bubble curve and the saturation temperature to be fitted using a linear relationship of pressure. The coefficients of these equations are shown in Equations 4.15, 4.16 and 4.17. These equations are used in the classification of the phase of the working fluid. Based on the phase, whether that be subcooled, saturated or superheated, a different relationship for temperature and density is used. The resultant curves are shown in Figure 4.4. The temperature curve describes the typical phase change of a pure fluid, whereas a function of only enthalpy, a linear increase in temperature is shown during subcooled and superheating. This is separated by the evaporation region of the working fluid. If pressure is disregarded, the temperature remains constant with changing enthalpy within this range. In accounting for pressure, a linear increase in temperature is shown in the Y direction. The density curve can be described similarly, however, a cubic equation is used to describe the fluid undergoing evaporation. These curves were not required to be normalised for the coefficients to be fitted. The curve fit for the subcooled region is shown by Equation 4.13 and the curve fit for the superheated region is shown by Equation 4.14. The remaining equations and graphs are shown in Appendix A: Working Fluid Fitted Correlations.

$$T_{wf} = (-2.42e^{-11}P + 0.0003)H + 1.11e^{-5}P + 49.47 \tag{4.13}$$

Where H and P are the subcooled enthalpy and pressure of the working fluid.

$$T_{wf} = (-1.85e^{-10}P + 0.00074)H + 1.24e^{-4}P - 293.8 \tag{4.14}$$

Where H and P are the superheated enthalpy and pressure of the working fluid.

The fitted coefficients for the bubble point are shown in Equation 4.15.

$$H_{wf_bubble} = 0.108P + 146628.9 \tag{4.15}$$

The fitted coefficients for the dew point are shown in Equation 4.16.

$$H_{wf_dew} = -0.022P + 512845.5 \tag{4.16}$$

The fitted coefficients for the saturated temperature are shown in Equation 4.17.

$$T_{wf_sat} = 2.67P + 11.2 \tag{4.17}$$

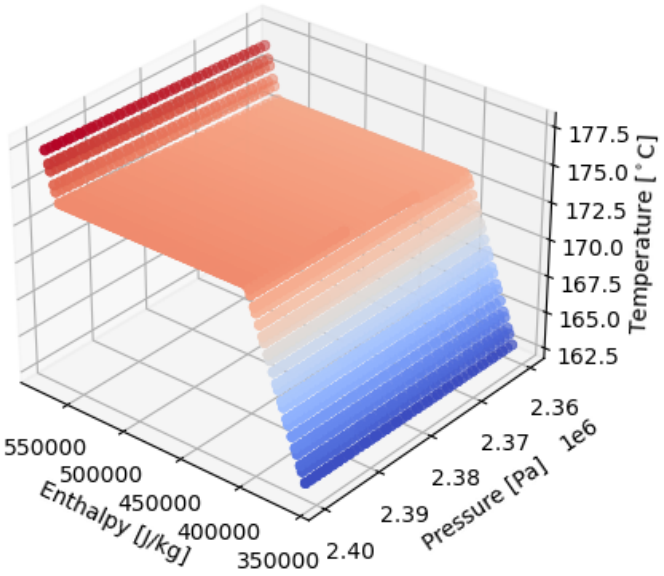

(A)

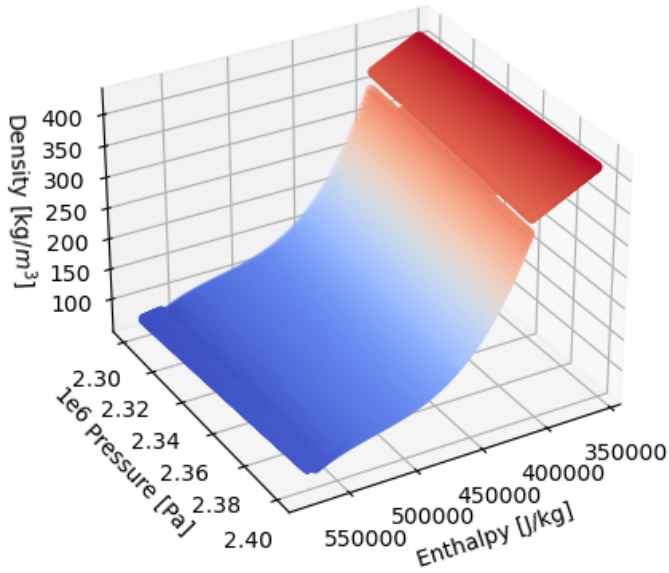

(B)

FIGURE 4.4: Prediction of temperature in (°C) in Figure A and density in kgm^{-3} in Figure B of n-pentane. Both correlations are in terms of enthalpy and pressure

The simplified geothermal vapour is a mixture of water and carbon dioxide. The composition is shown in Table 3.2. The inlet of the vapour is assumed to be saturated, therefore this limits the upper conditions of the vapour. The water vapour of this mixture undergoes condensation, resulting in a three-phase mixture of carbon dioxide vapour, remaining water vapour and liquid water, therefore a comparatively more complex model is required. During the condensation of the water vapour, sensible heat is lost due to the presence of carbon dioxide. Based on the characteristics of this curve, a power equation was used for temperature and density correlations in terms of enthalpy. As a function of pressure, both curves display a linear relationship in the P axis, shown in Figure 4.5. These curves were required to be normalised with the maximum and minimum enthalpies 2710071 J kg^{-1} and 772538 J kg^{-1} and pressures 13.14 *bar* and 12.55 *bar*. These ranges are based on the maximum and minimum plant conditions shown in the plant data. This was done to allow easier fitting of the coefficients. The coefficients are shown below in Equation 4.18.

$$T_v = (1.43P_n + 16.66)e^{-H_n(0.0025P_n - 0.054)} + 0.71P_n + 173.5 \tag{4.18}$$

Where P_n and H_n refer to the normalised pressure and normalised enthalpy, respectively. The density curve coefficients are shown in Appendix B: Geothermal Fluid Fitted Correlations.

The geothermal brine is assumed to be pure water. As the brine undergoes solely sensible cooling, a linear model of temperature and density in terms of enthalpy fits the relationship. The temperature and density also show a linear relationship as a function of pressure. The enthalpy and pressure are normalised to replicate the form of the geothermal vapour to allow for easier processing in Python. These values were normalised with enthalpies 816511 J kg^{-1} and 730288 J kg^{-1} and pressures 13.82 *bar* and 12.81 *bar*. These ranges are based on the maximum and minimum plant conditions shown in the plant data. The curve is shown in Figure 4.6. The coefficients are shown below in Equation 4.19.

$$T_l = (-0.0023P_n + 19.55)H_n - 0.011P_n + 172.5 \tag{4.19}$$

Where P_n and H_n refer to the normalised pressure and normalised enthalpy, respectively. The density curve coefficients are shown in Appendix B: Geothermal Fluid Fitted Correlations.

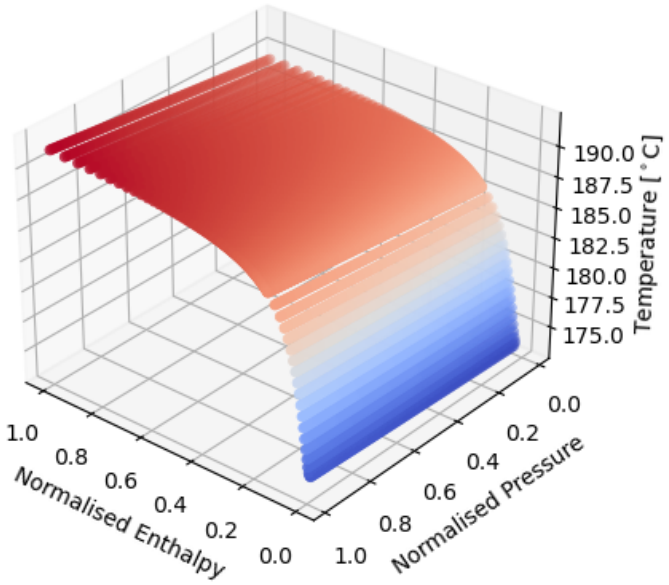

(A)

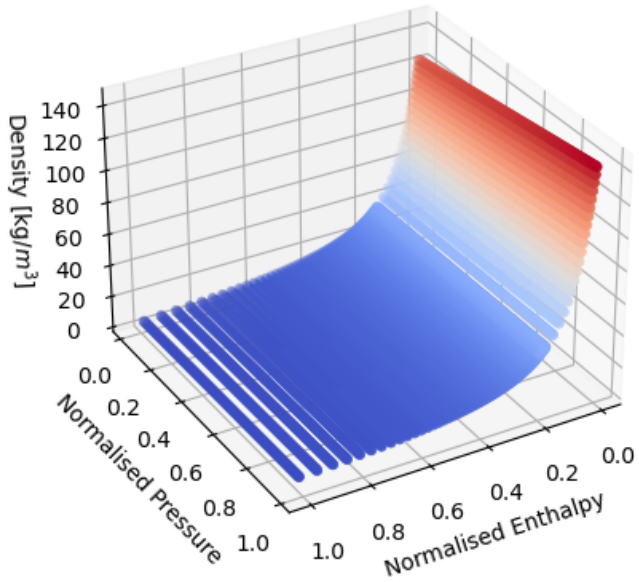

(B)

FIGURE 4.5: Prediction of temperature in (°C) in Figure A and density in kgm^{-3} in Figure B of the geothermal vapour. Both correlations are in terms of normalised enthalpy and pressure

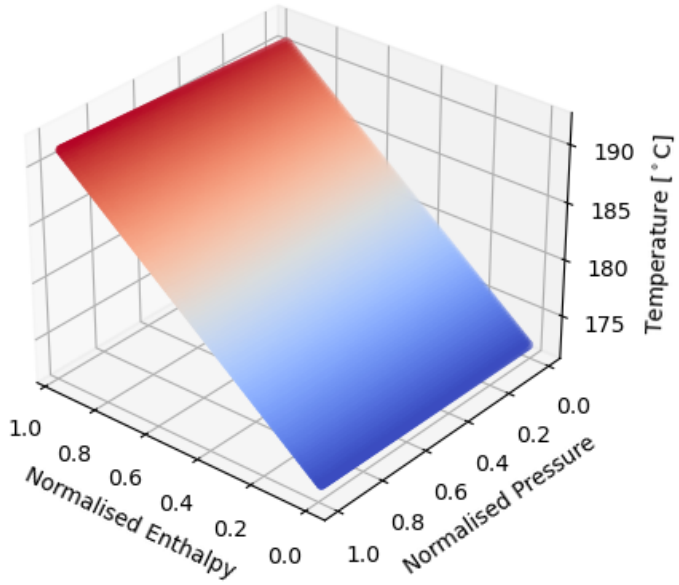

(A)

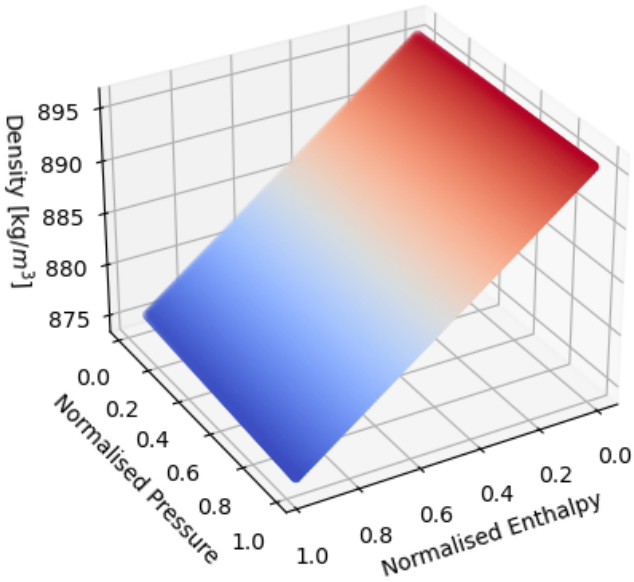

(B)

FIGURE 4.6: Prediction of temperature in (°C) in Figure A and density in kgm^{-3} in Figure B of the geothermal brine. Both correlations are in terms of normalised enthalpy and pressure

4.3.6.2 Validation of Curves

The validation of the temperature and density curves was carried out by comparing the predictions made by the fitted models with 10,000 data points values calculated through Aspen HYSYS. For the n-pentane working fluid, the Peng Robinson EOS could be used in CoolProp and Aspen HYSYS, however, the Helmholtz EOS is not available in Aspen HYSYS, therefore the CPA EOS was used. This would account for the small discrepancies between predictions of the aforementioned models and Aspen HYSYS. Regardless, adequate results are shown in the prediction of temperature and density, with an R^2 above 0.97 for all fluids. Results are shown in Table 4.5.

TABLE 4.5: Validation of data-driven correlations against data generated from Aspen HYSYS

Fluid Correlation	R^2	Units
T_l	0.990	$°C$
ρ_l	0.987	kgm^{-3}
T_{wf}	0.978	$°C$
ρ_{wf}	0.981	kgm^{-3}
T_v	0.986	$°C$
ρ_v	0.991	kgm^{-3}

4.3.7 Model Tuning and Steady State Validation

The model was tuned to the steady state data from Case 1 using the minimise module from SciPy integrate. Steady state results of the tuned First Principles (FP) model are shown in Table 4.6. Adequate predictions are shown in each stream outlet temperature. The model was then validated against the Case 2 data set, the results of which are shown in Table 4.7. During validation, an instability was noticed surrounding the power model fit for the temperature prediction of the vapour. This prediction showed an absolute error and percent error of 4.13$°C$ and 2.37%, respectively. Both the instability and the comparatively larger error is thought to be a result of the vapour cooling to a lower temperature than accounted for by this curve. This could be addressed by widening the applicable ranges of the temperature curve.

TABLE 4.6: Steady state validation of FP model against plant data from Case 1

Fluid Variable	Plant Data	FP Model	Error Abs.	Error (%)
$T_{wf_vap_out}$ (°C)	174.0	173.87	0.13	0.07
$T_{v_vap_out}$ (°C)	174.8	174.89	0.09	0.05
$T_{l_vap_out}$ (°C)	174.6	174.63	0.03	0.02

TABLE 4.7: Steady state validation of FP model against plant data from Case 2

Fluid Variable	Plant Data	FP Model	Error Abs.	Error (%)
$T_{wf_vap_out}$ (°C)	170.0	170.00	0.00	0.00
$T_{v_vap_out}$ (°C)	170.4	174.53	4.13	2.37
$T_{l_vap_out}$ (°C)	170.8	171.98	1.18	0.69

4.4 Dynamic Comparison

In order to transition the Aspen HYSYS vaporiser model into its dynamic state, pressure drops had to be introduced into the model, as a requirement for flow in Aspen HYSYS. As a result, small adjustments were made to tuning factors to facilitate this change. Changes were also made to the FP model in transitioning into dynamic conditions. One of the assumptions was that the predicted conditions of the shell-side of Section 3 could be approximated based on the average of inlet and outlet enthalpy. This was found to remove any disturbances expected in the vapour outlet temperature. Instead, only the outlet enthalpy was used for approximating the temperature and the density of the working fluid in Section 3 of the vaporiser. Two cases of 800 s were simulated, however, only 100 s to 600 s is displayed in Figure 4.7, to clearly show the step change. The Aspen HYSYS model is used as the standard to which the FP model is compared. In both cases there is good agreement between the models.

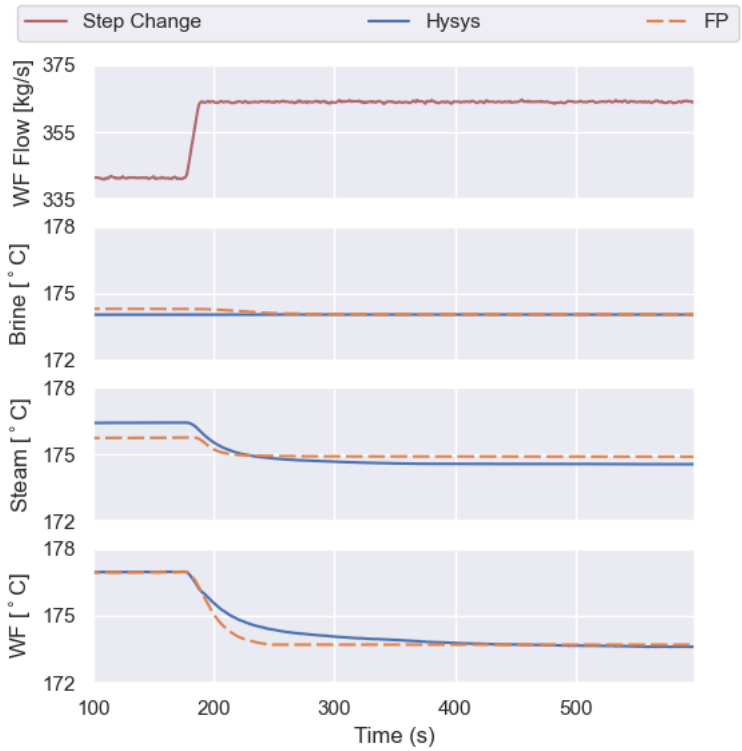

(A)

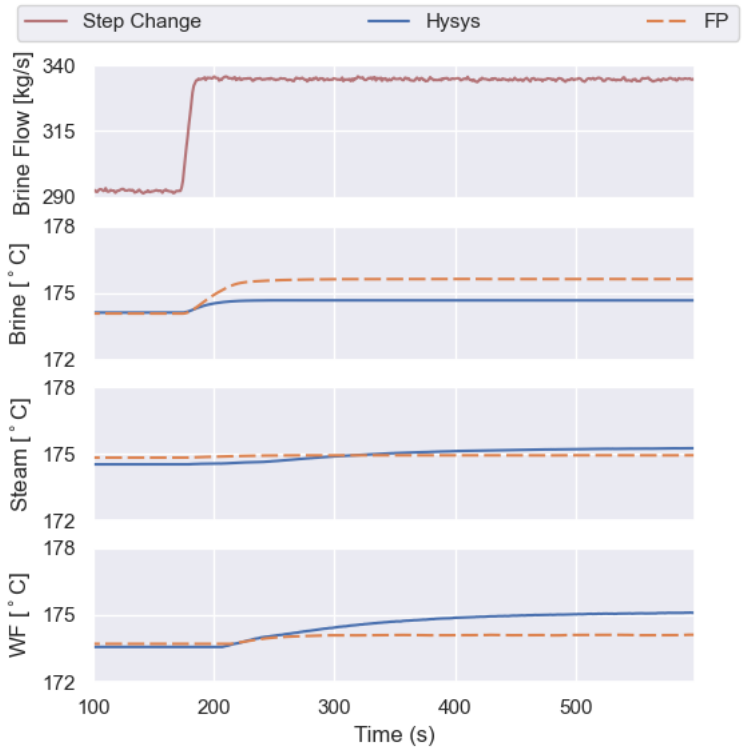

(B)

FIGURE 4.7: Step change of the working fluid (A) and brine (B) flow-rates and the temperature response of the vaporiser for the Aspen HYSYS model and the First Principles model

4.4.1 Working Fluid Step Change

To test the dynamic response of all the outlet streams of the vaporiser, the working fluid flow-rate was increased from 1230T/h to 1310T/h. This result is shown in Figure 4.7a, which displays the expected responses for each stream. The lack of response displayed in the brine outlet of the Aspen HYSYS model is a consequence of the method of calculation for heat transfer. As shown in Haydary, 2019, enthalpy balances and the LMTD approach are used to calculate heat transfer in Aspen HYSYS. Before and after the step change, the temperature of the working fluid leaving the brine heat exchanger is largely unaffected by the mass flow-rate step change. This is due to it undergoing evaporation. From inspection of the data, a $0.01°C$ increase of the brine outlet temperature can be seen at the time of the step change.

The FP model appears to show a comparatively faster response, which is most evident in the working fluid's response. The response of Aspen HYSYS, in addition to being slower, appears to be of a comparatively higher-order derivative. This is thought to result from the more comprehensive 'hold up' and pressure specifications used in Aspen HYSYS's heat exchanger model which mimics physical systems. This could be addressed by implementing more rigorous mass and momentum balances into the ODE or by tuning the model dynamically (Pili, Spliethoff, and Wieland, 2017; Huster et al., 2018).

When comparing the FP model against the outlet temperatures produced in Aspen HYSYS, a Root Mean Squared Error (RMSE) of $0.124°C$, $0.401°C$ and $0.250°C$ was shown for the brine, vapour and working fluid respectively. The mean average percentage error (MAPE) was 0.039%, 0.211% and 0.093% for brine, vapour and working fluid, respectively.

TABLE 4.8: Working fluid step change - Dynamic comparison between Aspen HYSYS model and FP model

Fluid Variable	RMSE.	MAPE%
$T_{wf_vap_out}(°C)$	0.2496	0.093%
$T_{v_vap_out}(°C)$	0.4009	0.211%
$T_{l_vap_out}(°C)$	0.1235	0.039%

4.4.2 Brine Step Change

A brine flow-rate step change from 1000T/h to 1200T/h was also tested. The dynamic response is shown in Figure 4.7b. The slight delay in response of the working fluid outlet temperature is a result of the change from a vapour fraction of approximately 0.98 to a fully vaporised outlet. This delay in increasing temperature is captured by both models. A very small increase was noted in the outlet vapour temperature of the FP model of approximately 0.01°C. Like the working fluid step change, the Aspen HYSYS model's response appears slower which reiterates that this model may be higher order. Though this is not displayed in the graph, the working fluid response of the Aspen HYSYS model does reach steady state.

The outlet brine and working fluid temperatures of the FP model display an offset, which is shown most evidently in Figure 4.7b, although is noticeable prior to the step change of the working fluid in Figure 4.7a. This could be addressed by additional tuning, particularly so around the brine step change. Comparing the FP outlets against the outlet temperatures produced in Aspen HYSYS, an RMSE of 0.848°C, 0.279°C and 0.764°C were obtained for the brine, vapour and working fluid, respectively. The MAPE was 0.442%, 0.152% and 0.378% for brine, vapour and working fluid, respectively.

TABLE 4.9: Brine step change - Dynamic comparison between Aspen HYSYS model and FP model

Fluid Variable	RMSE.	MAPE%
$T_{wf_vap_out}(^\circ C)$	0.764	0.378%
$T_{v_vap_out}(^\circ C)$	0.279	0.152%
$T_{l_vap_out}(^\circ C)$	0.848	0.442%

4.5 Conclusions

Based on this chapter's analysis, both the models produced in this thesis have shown an adequate prediction accuracy at the two steady state cases of the plant. The temperature predictions were shown for the outlet geothermal brine, vapour and working fluid of the Aspen HYSYS model with a percent error of 0.02%, 0.06% and 0.04%, respectively, for the validation with Case 2, while the FP model showed a percent error of 0.69%, 2.37% and 0.003%, respectively. The range of applicability of the FP model could be improved by widening the range of conditions used in fitting the

empirical correlations for the temperature of the geothermal vapour. Both models could be further improved by comparing results with an operational data set in order to validate these models dynamically.

Based on the current analysis, and considering the Aspen HYSYS model as the "de facto" for comparison, the First Principles model is able to replicate the behaviour of the Aspen HYSYS model with reasonable accuracy. Improvements could be made to the FP model response to more resemble the behaviour of the Aspen HYSYS model by implementing more rigorous mass balances and tuning the model dynamically. It is also thought that the dynamic response could be improved through the application of the two-volume methodology. This would better approximate evaporation and the mixing that would realistically occur in the vaporiser shell. However, application of this would require further segmentation into three volumes as the vaporiser inlet is subcooled to a significant degree.

The plant model which was developed showed good predictions of the vaporiser outlets, however, streams surrounding the NCG pre-heater showed significant errors up to 29% when compared with plant data. This is thought to result from the difficulties of the EOS replicating the state behaviour of a gaseous and liquid water and carbon dioxide gas mixture. Further research is required to assess other EOS options or to potentially develop a new EOS tailored to carbon dioxide and water compositions seen in geothermal applications.

The models developed in this thesis and the software tools used will be compared in Chapter 5 based on their performance, availability, ease of use and model fidelity.

Chapter 5

Model Comparison

5.1 Preface

This chapter covers a comparison between the models developed in this thesis, and the software tools used in model development. The comparison criteria are based on Alford, 2021. This comparison is also extended to the model fidelity framework outlined by Yu et al., 2022.

5.2 Comparison Criteria

The comparison criteria for software tools used in model development are based on (Alford, 2021): this includes the model performance and availability of the software. The comparison criteria are also extended to include the aforementioned model fidelity framework from Section 1.4 and the ease of use of the modelling software.

5.2.1 Performance

The model performance considers prediction accuracy and the processing time required. The prediction accuracy is arguably the most important attribute of these models. The steady state results for Case 1 and Case 2 are shown in Tables 5.1 and 5.2. In Case 1, both models perform functionally the same, with a minuscule improvement shown by the FP model. However, in Case 2, the Aspen HYSYS model shows a lower error. This is largely a result of the error in the vapour outlet temperature, which is potentially caused by the fitted temperature curve. Extending this comparison to the dynamic step changes, the highest RMSE found was in the brine outlet temperature prediction. This error was 0.848 °C when compared with the Aspen Hysys model's prediction.

The processing speed is also considered as this is required for real-time simulation. An approximate value was measured using Google's stopwatch for the Aspen HYSYS model which required 93.09 +/- 1 timed seconds to simulate 830 simulated seconds. The same simulation was tested using the FP model which was measured using Python's built-in time module. This required 80.09 seconds. Based on these results, both models would be capable of simulating the vaporiser parallel to the system, with the FP model running slightly faster.

TABLE 5.1: Error of the Aspen HYSYS vaporiser model for steady state Case 1 and 2

Aspen HYSYS Model	Case 1		Case 2	
	Error Abs.	Error (%)	Error Abs.	Error (%)
$T_{wf_vap_out}$	0.03	0.02	0.07	0.04
$T_{v_vap_out}$	0.17	0.1	0.10	0.06
$T_{l_vap_out}$	0.05	0.03	0.03	0.02

TABLE 5.2: Error of the First Principles vaporiser model for steady state Case 1 and 2

First Principles Model	Case 1		Case 2	
	Error Abs.	Error (%)	Error Abs.	Error (%)
$T_{wf_vap_out}$	0.13	0.07	0.00	0.00
$T_{v_vap_out}$	0.09	0.05	4.13	2.13
$T_{l_vap_out}$	0.03	0.02	1.18	0.69

5.2.2 Availability

The availability considers the accessibility and the monetary investment of these software tools. Python and CoolProp are both available worldwide at no cost, while an Aspen HYSYS dynamic licence, though also globally available, costs approximately 85% of a process engineering graduate's annual salary in New Zealand.

5.2.3 Ease of Use

This section considers the difference in time, effort and skill requirements of developing each model. Of the entire FP model, a relatively small percentage of the written code is used for the calculation of heat transfer, whereas the remaining code is used in setting up the thermodynamic properties and state variables. This set-up includes the developed empirical equations and CoolProp. This differs from the Aspen HYSYS model which has a wide range of easily accessible thermodynamic property packages.

In calculating the heat transfer, Aspen HYSYS allows the use of built-in unit operations, however, for this case it does not accommodate multiple tube-set heat exchangers. Using two heat exchangers in series allows the ability to replicate this vaporiser's configuration. This highlights a difficulty in Aspen HYSYS if modelling a unique unit operation. An alternative is to use the inbuilt, Excel-based formats that could add flexibility to the unit operations. Using Python allows for a large degree of flexibility as the differential equations are formulated on First Principles equations. This allows the model to easily replicate unique equipment that is not accounted for in available unit operations.

In the development of both models, a graduate chemical engineering background would be necessary. In addition to this, the Python model would require an intermediate level of coding skills which would have a significant impact on the time taken in this model's development. In this case, with minimal prior coding experience, it is thought to have taken a four-month period in development of the First Principles model. Yet, using Aspen HYSYS, the vaporiser model, excluding the plant model, was able to be developed in less than a week.

The assured robustness of either software is also a point of comparison. Developing the FP model as an individual, the quality assurance of the model is significantly less than that of a well-established tool such as Aspen HYSYS. The latter is developed by a team of industry professionals recognised as the industry standard for process simulation.

5.2.4 Model Fidelity

As outlined in section 1.4, the model fidelity framework includes three distinct attributes of a Digital Twin: looks-like, behaves-like and connects to. Both models developed have been validated against multiple steady state data points and are capable of modelling dynamically. These models therefore would be classified as 3-D in the behaves-like attribute.

The Aspen HYSYS model would be considered a 2-D visual representation of the vaporiser. A visual process flow diagram is used as an interactive medium in addition to the vaporiser specific dimensions being used in the model. The FP model also uses vaporiser specific dimensions, and a coordinate system of both horizontal and vertical dimensions: this would therefore be considered a 2-D in the visual-likeness attribute.

Neither model has an automatic connection between model and plant, and therefore would be considered a digital model. A proposed connection could be developed between the FP vaporiser model and the plant model developed in Aspen HYSYS. To justify this other than as a proof of concept, the performance in both prediction accuracy and processing speed would have to be significantly better in the FP vaporiser model than the Aspen HYSYS vaporiser model. In this current iteration this is not the case.

These results are summarised in Table 5.3.

TABLE 5.3: Summary of the comparisons of the First Principles and Aspen HYSYS model attributes

Model Attribute	**Aspen HYSYS**	**First Principles**
Average Prediction Error of Steady State Case 1 and 2	0.084 & 0.065	0.082 & 1.773
Simulation Speed (s)	93.09	80.09
Availability	Available worldwide	Available worldwide
Software Cost	85% of a graduate process engineer's annual salary	Freely available
Set-up (thermodynamic properties)	Built-in to the software	Set-up using CoolProp
Flexibility of Heat Transfer	Less flexible, easily used if the unit operation is available	As the heat transfer equation is formulated high degree of flexibility
Development Time (Estimate)	1 week	4 months
Quality Assurance/Robustness	Tested commercially by a professional team of people	Tested by one person
Behaves-like	3D	3D
Looks-like	2D	2D
Connects-to	1D	1D

5.3 Conclusions

In summary, the suitability of Aspen HYSYS and Python modelling tools were compared. Both models showed similar predictions in both steady state cases. The time investment for the FP model is significantly higher than for the Aspen HYSYS model. This is largely a result of the amount of thermodynamic set-up required in the FP model, while having this readily available in the Aspen HYSYS model. However, a dynamic licence of Aspen HYSYS for a single user is approximated at 85% of a New Zealand process engineering graduate's annual salary. This highlights a trade-off between time and monetary investments by the modelling software used.

The fidelity of each of the modelling tools is comparable. Both models are considered as 3-D in the behaves-like attribute, and both models are manually input with data, therefore are considered digital models. These models would also be considered 2-D in visual representation due to their vaporiser specific dimensions and coordinate system of the vaporiser.

Chapter 6 covers the overall conclusions and recommendations of this work.

Chapter 6

Conclusions

This thesis develops and compares various modelling techniques and the software tools used in their development. The subject of these models was an industrial-scale vaporiser with multiple tube-sets, which is an essential part of an ORC cycle in a binary geothermal plant. This was used to further understand the key strengths and limitations of the software tools used, and the model development process. As part of the Ahuora research programme, this work will aid the development and understanding of Digital Twins for New Zealand industries.

Firstly, a plant model of the ORC cycle was developed in Aspen HYSYS, which was used as a tool in the development of the vaporiser models. Additionally, as future work, this could be used in the development of a Digital Twin for a virtual plant. The vaporiser model was developed in Aspen HYSYS as part of the plant model, however, the former was separately transitioned into a dynamic state in which additional tuning was required. A unique approach had to be taken, utilising two heat exchangers in series to model the vaporiser. These models were validated against two sets of steady state data.

Secondly, a First Principles-based model of the vaporiser was developed in Python using the Discretised approach. This required segmentation of the model into three sections, each corresponding to a separate pass of the tubes. In order to improve processing speeds, empirical correlations were developed for temperature and density based on data generated from CoolProp. This vaporiser model was validated against two sets of steady state data.

Each of the models described, showed adequate predictions at multiple steady state conditions. However, of the vaporiser models, the Aspen HYSYS model performed slightly better with a percent error of 0.02%, 0.06% and 0.04%, for the temperatures of the outlet geothermal brine, vapour and working fluid, respectively. The

FP model showed a percent error of 0.69%, 2.37% and 0.003% for the same streams, respectively. The plant model showed reasonable predictions around most of the key streams, however, a sizable error was shown in the non-condensable gas leaving the system. This is likely to be a result of the equations of state used for this stream, and its difficulty in replicating behaviour of fluids with higher CO_2 mole fraction. The dynamic behaviour of the vaporiser models is shown, where the First Principles model is able to replicate the behaviour of the Aspen HYSYS model for most streams. However, differences were noted in the differential order of the models.

A comparison was made between models and the tools used in their development based on attributes of performance, availability, ease of use and model fidelity. As described, there were slight differences in prediction performance and in processing speeds. For the availability and ease of use of these tools, a trade-off would need to be made in deciding which modelling software to use, weighing monetary investment in using Aspen HYSYS against the time investment in using Python. In terms of model fidelity, the First Principles model and Aspen HYSYS model would be categorised as a 3-2-1D model in terms of behaves-like, looks-like and connects-to attributes.

6.1 Future Work

Through this thesis' investigation into geothermal vaporiser modelling, various areas for potential improvements and future research arose. These are:

Improved Aspen HYSYS Model: The areas of improvement for the Aspen HYSYS model were its dynamic validation against plant data and further investigation into the equations of state. Further validation of the Aspen HYSYS model against dynamic plant data would be beneficial in tuning the model's dynamic response.

Improved First Principles Model: The areas of improvement for the First Principles model were its dynamic response and applicable ranges of the temperature model for the geothermal vapour. Two improvements could address the dynamic response: these are the use of the two-volume modelling approach, and the dynamic tuning of the model. The two-volume approach involves a significantly more complex mass balance of the shell, directly approximating evaporation rates and therefore mass flow between each volume. Additionally, further validation and tuning

with dynamic plant data could be used to improve the model's dynamic response.

Another potential area of improvement is the inaccuracies of the model at comparatively lower temperatures. The inaccuracies are thought to be a result of the temperature relationship for the geothermal vapour, and could be addressed by fitting the curve to wider temperature ranges.

Black Box Model Comparison: In addition, a Black Box model comparison would be useful in widening the range of models developed. Based on the literature reviewed in Section 2.5, hitherto only one industrial-scale Black Box model has been developed which shows promising results.

Implementing One-way Connection: The development of a one-way connection between the First Principles model and the Aspen HYSYS plant model would be useful as a step towards a Digital Twin and allowing a plant model with more flexibility in vaporiser modelling. This would address the gap seen in the literature regarding a lack of Digital Shadows and Digital Twins of ORCs.

Chapter 7

Appendices

Appendix A: Working Fluid Fitted Correlations

The fitted coefficients for the density of the working fluid (normal pentane) are shown in Equations 7.1, 7.3 and 7.4. These correspond to the evaporating, subcooled and superheated regions of the working fluid.

$$\rho_{wf_evap} = (-2.37e^{-20}P - 5.87e^{-14})H^3 + (5.97e^{-14}P - 3.82e^{-8})H^2 \tag{7.1}$$

$$+ (-4.35e^{-8}P + 0.0089)H + 0.0099P - 6798 \tag{7.2}$$

$$\rho_{wf_subcooled} = (-7.11e^{-11}P - 0.0009)H + 4.4e^{-5}P + 677 \tag{7.3}$$

Where H and P are the sub-cooled enthalpy and pressure of the working fluid.

$$\rho_{wf_superheat} = (-5.7e^{-10}P + 0.001)H + 0.00038P - 637.1 \tag{7.4}$$

Where H and P are the superheated enthalpy and pressure of the working fluid.

The bubble point curve is shown in Figure 7.1.

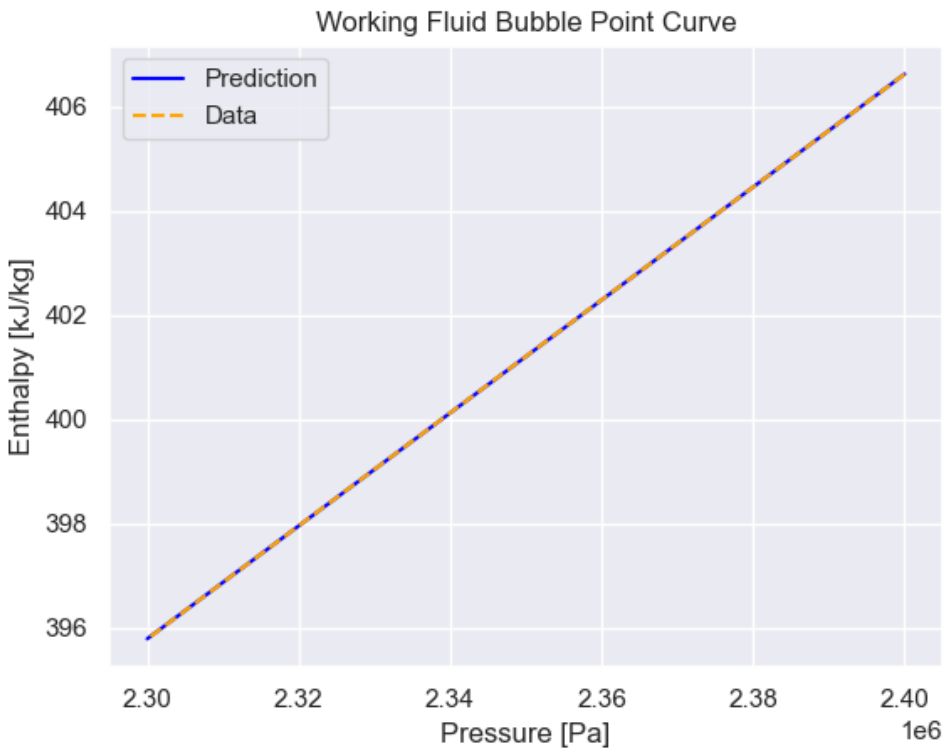

FIGURE 7.1: Bubble point curve of the working fluid fitted against pressure

The dew point curve is shown in Figure 7.2.

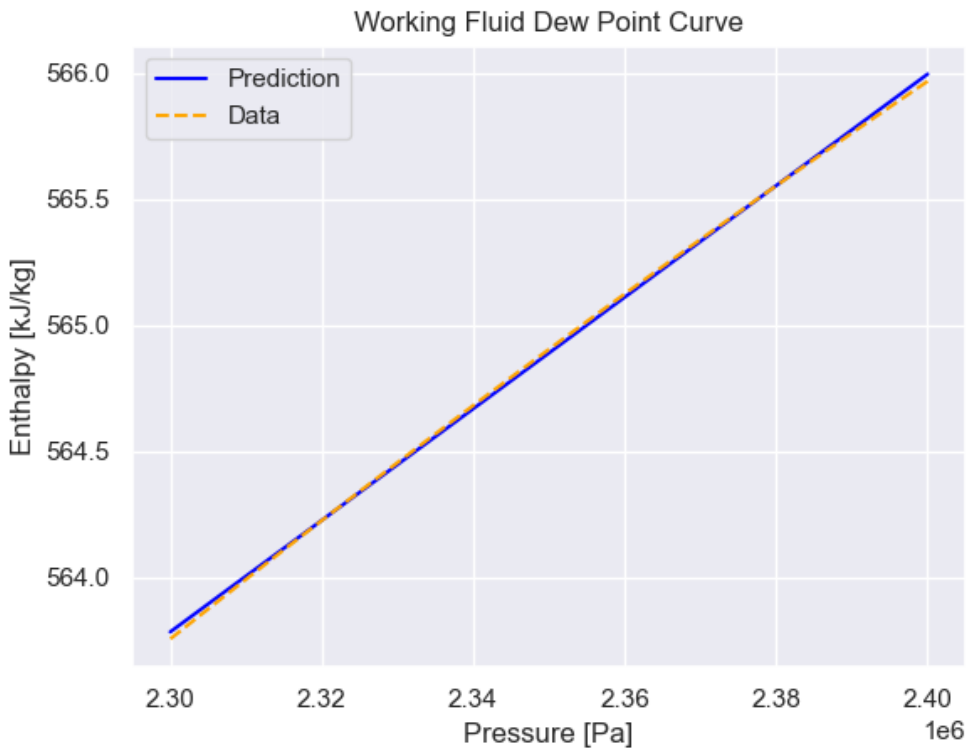

FIGURE 7.2: Dew point curve of the working fluid fitted against pressure

The saturated temperature curve is shown in Figure 7.3.

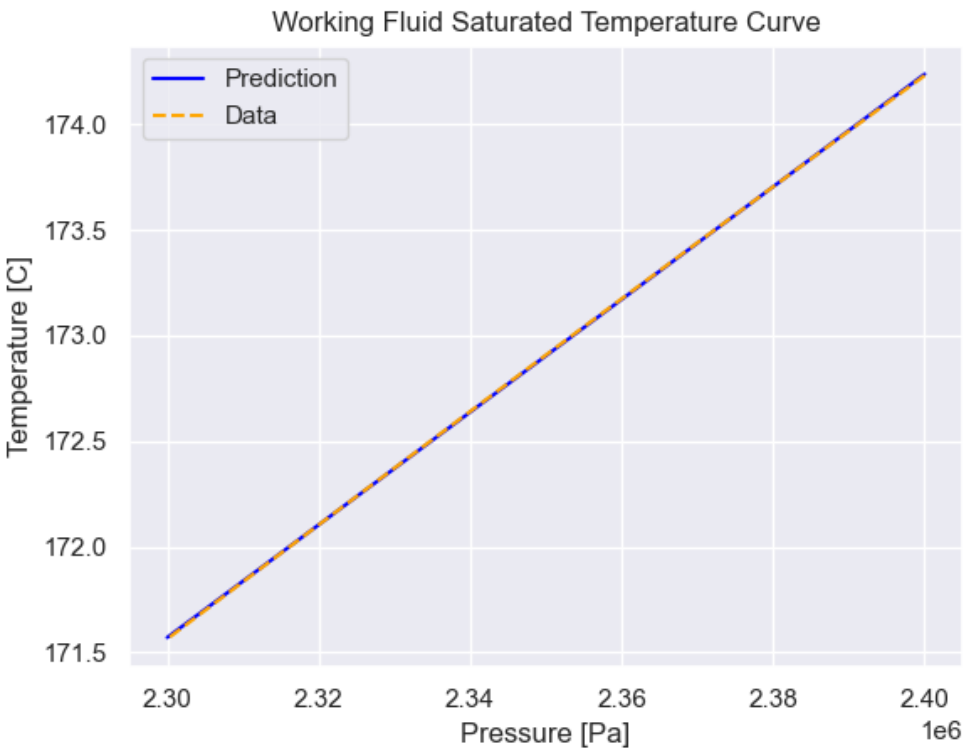

FIGURE 7.3: Saturated temperature curve of the working fluid fitted against pressure

Appendix B: Geothermal Fluid Fitted Correlations

The fitted coefficients for the density of the geothermal vapour are shown in Equation 7.5.

$$\rho_v = (-12.4P_n - 117.8)e^{-H_n(0.0025P_n - 0.063)} + 12.2P_n + 116.9 \tag{7.5}$$

Where P_n and H_n refer to the normalised pressure and normalised enthalpy respectively.

The fitted coefficients for the density of the geothermal brine are shown in Equation 7.6.

$$\rho_l = (-0.013P_n - 21.3)H_n + 0.084P_n + 884.3 \tag{7.6}$$

Where P_n and H_n refer to the normalised pressure and normalised enthalpy respectively.

Appendix C: First Principles Paper Summary

The table summary of First Principles papers is shown in 7.1.

TABLE 7.1: First Principles paper summary where MD and MS stand for Modelica Dymola, and MATLAB Simulink environments respectively. NA is used where no validation data or software is provided

Model Type	Validation Data	Software	Reference
Steady State	Model Based	NA	Hettiarachchi et al., 2007
Steady State	NA	MD	Wei et al., 2007
Dynamic	Lab	MD	Wei et al., 2008
Steady State	NA	NA	Franco et al., 2009
Steady State	NA	NA	Dai et al., 2009
Dynamic	Industrial Plant	gProms	Sohel et al., 2010
Dynamic	Industrial Plant	NA	Sun et al., 2011
Dynamic	NA	MD	Quoilin et al., 2011
Dynamic	Lab	NA	Zhang et al., 2012
Steady State	Model Based	EES	Khennich et al., 2012
Steady State	NA	EES	Meyer et al., 2013
Steady State	NA	Other	El-Emam et al., 2013
Steady State	NA	MATLAB	Wang et al., 2013
Dynamic	Lab	MS	Feru et al., 2014
Dynamic	Lab	MS	Zhang et al., 2014
Steady State	NA	Aspen Plus	Lv et al., 2014
Dynamic	Industrial Plant	MS	Mazzi et al., 2015
Dynamic	Lab	VMG Sim	Lie, 2015
Dynamic	NA	MATLAB	Grelet et al., 2015
Steady State	NA	EES	Taylor, 2015
Dynamic	Industrial Plant	VMG Sim	Proctor et al., 2016
Dynamic	Lab	MS	Seitz et al., 2016
Dynamic	NA	NA	Shi et al., 2016
Dynamic	Industrial Plant	MD	Pili et al., 2017
Dynamic	Lab	gProms	Schilling et al., 2017
Dynamic	Lab	MS	Koppauer et al., 2017
Dynamic	Lab	MS	Xu et al., 2017

Continuation of Table 7.1.

Model Type	Validation Data	Software	Reference
Dynamic	Lab	Aspen Plus	Kuboth et al., 2017
Dynamic	Lab	MATLAB	Liu et al., 2017
Dynamic	Lab	GT Suite	Marchionni et al., 2017
Dynamic	Model Based	MATLAB	Lakhani et al., 2017
Dynamic	NA	NA	Jolevski et al., 2017
Dynamic	Pilot Plant	NA	Wang et al., 2017
Steady State	NA	NA	Gullapalli, 2017
Steady State	NA	Aspen Plus	Rajabloo, 2017
Dynamic	Lab	MD	Ni et al., 2018
Dynamic	Lab	GT Suite	Zhao et al., 2018
Dynamic	Lab	gProms	Huster et al., 2018r
Dynamic	NA	MS	Li et al., 2018
Steady State	NA	NA	Jang et al., 2018
Steady State	NA	Aspen Plus	Nur et al., 2018
Steady State	NA	NA	Sun et al., 2018
Steady State	NA	EES	Bellos et al., 2018
Dynamic	Lab	MD	Zhang et al., 2019
Dynamic	Lab	MS	Carraro et al., 2019
Dynamic	NA	MD	Jiménez-Arreola et al., 2019
Steady State	Model Based	MATLAB	Wang et al., 2019
Steady State	Model Based	MATLAB	Luo et al., 2019
Dynamic	Lab	MD	Pili et al., 2020
Dynamic	Lab	MS	Xu et al., 2020
Steady State	Industrial Plant	EES	Altun et al., 2020
Steady State	NA	Aspen HYSYS	Hidayah et al., 2020
Steady State	NA	NA	Petrollese et al., 2020
Steady State	NA	MATLAB	Feng et al., 2020
Dynamic	Model Based	MS	Cao et al., 2021
Steady State	NA	MS	Liu et al., 2020

Appendix D: Black Box Paper Summary

The table summary of Black Box papers is shown in 7.2.

TABLE 7.2: Black Box paper summary where NA is used shown when no validation data or software is provided

Model Type	Validation Data	Software	Reference
Steady State	No Source	MATLAB	Arslan et al., 2011
Dynamic	Model Based	MATLAB	Chowdhury et al., 2015
Dynamic	Model Based	NA	Zhang et al., 2012
Steady State	Model Based	MATLAB	Massimiani et al., 2017
Steady State	No Source	NA	Kovacı et al., 2017
Steady State	Lab	NA	Dong et al., 2018
Dynamic	Model Based	NA	Chowdhury et al., 2018
Dynamic	Lab	NA	Yang et al., 2018
Steady State	Model Based	MATLAB	Kılıç et al., 2019
Steady State	Lab	MATLAB	Khosravi et al., 2019
Dynamic	Lab	Python	Palagi et al., 2019
Steady State	Model Based	MATLAB	Schweidtmann et al., 2019
Steady State	Model Based	MATLAB	Huster et al., 2019
Steady State	Model Based	MATLAB	Zhi et al., 2019
Dynamic	Lab	NA	Enayatollahi et al., 2020
Steady State	Model Based	Python	Wang et al., 2020
Steady State	Lab	NA	Feng et al., 2020
Steady State	Model Based	MATLAB	Huster et al., 2020
Steady State	Lab	Python	Mert et al., 2020
Steady State	Lab	MATLAB	Yan et al., 2021
Steady State	Model Based	NA	Peng et al., 2021
Dynamic	Industrial Plant	NA	Liu et al., 2021

References

Alford, Molly (2021). "A Literature Review of Tools and Software for Process Digital Twins for Decarbonization". In: Unpublished Work.

Altun, A. F. and M. Kilic (Apr. 2020). "Thermodynamic performance evaluation of a geothermal ORC power plant". In: *Renewable Energy* 148, pp. 261–274. ISSN: 18790682. DOI: 10.1016/j.renene.2019.12.034.

Arslan, Oguz and Ozge Yetik (Dec. 2011). "ANN based optimization of supercritical ORC-Binary geothermal power plant: Simav case study". In: *Applied Thermal Engineering* 31 (17-18), pp. 3922–3928. ISSN: 13594311. DOI: 10.1016/j.applthermaleng.2011.07.041.

Aspen Technology (2013). *Aspen Physical Property Methods*. URL: http://www.aspentech.com.

Bajpai, Pratima (2018). *Biotechnology for Pulp and Paper Processing*. 2nd.

Bell, Ian H., Jorrit Wronski, Sylvain Quoilin, and Vincent Lemort (Feb. 2014). "Pure and pseudo-pure fluid thermophysical property evaluation and the open-source thermophysical property library coolprop". In: *Industrial and Engineering Chemistry Research* 53 (6), pp. 2498–2508. ISSN: 08885885. DOI: 10.1021/ie4033999.

Bellos, Evangelos and Christos Tzivanidis (Jan. 2018). "Investigation of a hybrid ORC driven by waste heat and solar energy". In: *Energy Conversion and Management* 156, pp. 427–439. ISSN: 01968904. DOI: 10.1016/j.enconman.2017.11.058.

Calise, Francesco, Adriano Macaluso, Pasquale Pelella, and Laura Vanoli (Dec. 2018). "A comparison of heat transfer correlations applied to an Organic Rankine Cycle". In: *Engineering Science and Technology, an International Journal* 21 (6), pp. 1164–1180. ISSN: 2215-0986. DOI: 10.1016/J.JESTCH.2018.09.009.

Cao, Liyan, Jiangfeng Wang, Yi Yang, Yaxiong Wang, Hang Li, Juwei Lou, Qiqi Rao, and Yan Li (Jan. 2021). "Dynamic analysis and operation simulation for a combined cooling heating and power system driven by geothermal energy". In: *Energy Conversion and Management* 228. ISSN: 01968904. DOI: 10.1016/j.enconman.2020.113656.

Carraro, Gianluca, Sergio Rech, Andrea Lazzaretto, Giuseppe Toniato, and P. Danieli (Oct. 2019). "Dynamic simulation and experiments of a low-cost small ORC unit for market applications". In: *Energy Conversion and Management* 197. ISSN: 01968904. DOI: 10.1016/j.enconman.2019.111863.

Carta, Giorgio (2021). *Convective Heat Transfer*. First edition. McGraw-Hill Education. ISBN: 9781264266678. URL: https://www.accessengineeringlibrary.com/content/book/9781264266678/chapter/chapter6.

Cavallini, Alberto, Davide Del Col, Luca Doretti, Marko Matkovic, Luisa Rossetto, Claudio Zilio, and Giuseppe Censi (Sept. 2006). "Condensation in Horizontal Smooth Tubes: A New Heat Transfer Model for Heat Exchanger Design". In: *Heat Transfer Engineering* 27 (8). doi: 10.1080/01457630600793970, pp. 31–38. ISSN: 0145-7632. DOI: 10.1080/01457630600793970. URL: https://doi.org/10.1080/01457630600793970.

Cayer, Emmanuel, Nicolas Galanis, Martin Desilets, Hakim Nesreddine, and Philippe Roy (2009). "Analysis of a carbon dioxide transcritical power cycle using a low temperature source". In: *Applied Energy* 86 (7-8), pp. 1055–1063. ISSN: 03062619. DOI: 10.1016/j.apenergy.2008.09.018.

Chowdhury, Jahedul Islam, Bao Kha Nguyen, and David Thornhill (2015). "Modelling of evaporator in waste heat recovery system using finite volume method and fuzzy technique". In: *Energies* 8 (12), pp. 14078–14097. ISSN: 19961073. DOI: 10.3390/en81212413.

Chowdhury, Jahedul Islam, Bao Kha Nguyen, David Thornhill, Yukun Hu, Payam Soulatiantork, Nazmiye Balta-Ozkan, and Liz Varga (Apr. 2018). "Fuzzy nonlinear dynamic evaporator model in supercritical organic Rankine cycle waste heat recovery systems". In: *Energies* 11 (4). ISSN: 19961073. DOI: 10.3390/en11040901.

Colucci, Vitantonio, Daniele Fiaschi, Martina Leveni, Giampaolo Manfrida, and Lorenzo Talluri (2019). "Thermodynamic model of geothermal resources for low-medium temperatures energy conversion process optimisation". In: *Chemical Engineering Transactions* 74, pp. 1213–1218. ISSN: 22839216. DOI: 10.3303/CET1974203.

Cooper, M. G. (Jan. 1984). "Heat Flow Rates in Saturated Nucleate Pool Boiling-A Wide-Ranging Examination Using Reduced Properties". In: *Advances in Heat Transfer* 16 (C), pp. 157–239. ISSN: 0065-2717. DOI: 10.1016/S0065-2717(08)70205-3.

Dai, Yiping, Jiangfeng Wang, and Lin Gao (Mar. 2009). "Parametric optimization and comparative study of organic Rankine cycle (ORC) for low grade waste heat recovery". In: *Energy Conversion and Management* 50 (3). Genetic algorithm used to optimise the thermodynamic models

, pp. 576–582. ISSN: 01968904. DOI: 10.1016/j.enconman.2008.10.018.

DiPippo, Ronald (2005a). *Chapter 17 - Heber Binary Plants Imperial Valley, California, USA*. Ed. by Ronald DiPippo. Elsevier Science, pp. 371–380. ISBN: 978-1-85617-474-9. DOI: https://doi.org/10.1016/B978-185617474-9/50050-9. URL: https://www.sciencedirect.com/science/article/pii/B9781856174749500509.

— (2005b). *Chapter 8 - Binary Cycle Power Plants*. Ed. by Ronald DiPippo. Elsevier Science, pp. 163–196. ISBN: 978-1-85617-474-9. DOI: https://doi.org/10.1016/B978-185617474-9/50040-6. URL: https://www.sciencedirect.com/science/article/pii/B9781856174749500406.

— (2016). *Chapter 1 - Geology of Geothermal Regions*. Ed. by Ronald DiPippo. Fourth Edition. Butterworth-Heinemann, pp. 3–22. ISBN: 978-0-08-100879-9. DOI: https://doi.org/10.1016/B978-0-08-100879-9.00001-X. URL: https://www.sciencedirect.com/science/article/pii/B978008100879900001X.

Dobson, M K and J C Chato (Feb. 1998). "Condensation in Smooth Horizontal Tubes". In: *Journal of Heat Transfer* 120 (1), pp. 193–213. ISSN: 0022-1481. DOI: 10.1115/1.2830043. URL: https://doi.org/10.1115/1.2830043.

Dong, Shengming, Yufeng Zhang, Zhonglu He, Na Deng, Xiaohui Yu, and Sheng Yao (Feb. 2018). "Investigation of Support Vector Machine and Back Propagation Artificial Neural Network for performance prediction of the organic Rankine cycle system". In: *Energy* 144, pp. 851–864. ISSN: 03605442. DOI: 10.1016/j.energy.2017.12.094.

Dong, Shoulong (2020). "Design of Organic Rankine Cycle (ORC) Systems Using Knowledge-Based Approaches". PhD Thesis. University of Auckland.

EECA (2019). *Process Heat in New Zealand: Overview*. URL: https://www.mbie.govt.nz/building-and-energy/energy-and-natural-resources/low-emissions-economy/process-heat-in-new-zealand/.

El-Emam, Rami Salah and Ibrahim Dincer (2013). "Exergy and exergoeconomic analyses and optimization of geothermal organic Rankine cycle". In: *Applied Thermal Engineering* 59 (1-2), pp. 435–444. ISSN: 13594311. DOI: 10.1016/j.applthermaleng.2013.06.005.

Enayatollahi, Hamid, Peter Fussey, and Bao Kha Nguyen (Oct. 2020). "Modelling evaporator in organic Rankine cycle using hybrid GD-LSE ANFIS and PSO ANFIS techniques". In: *Thermal Science and Engineering Progress* 19. ISSN: 24519049. DOI: 10.1016/j.tsep.2020.100570.

Farid, Mohammed M (2010). *Mathematical Modeling of Food Processing*. DOI: https://doi.org/10.1201/9781420053548.

Feng, Yong qiang, Yu Zhuang Liu, Xin Wang, Zhi Xia He, Tzu Chen Hung, Qian Wang, and Huan Xi (Dec. 2020). "Performance prediction and optimization of an organic Rankine cycle (ORC) for waste heat recovery using back propagation neural network". In: *Energy Conversion and Management* 226. ISSN: 01968904. DOI: 10.1016/j.enconman.2020.113552.

Feru, Emanuel, Frank Willems, Bram de Jager, and Maarten Steinbuch (2014). "Modeling and control of a parallel waste heat recovery system for Euro-VI heavy-duty diesel engines". In: *Energies* 7 (10), pp. 6571–6592. ISSN: 19961073. DOI: 10.3390/en7106571.

Franco, Alessandro and Marco Villani (Dec. 2009). "Optimal design of binary cycle power plants for water-dominated, medium-temperature geothermal fields". In: *Geothermics* 38 (4), pp. 379–391. ISSN: 03756505. DOI: 10.1016/j.geothermics.2009.08.001.

Fu, Ben Ran, Yuh Ren Lee, and Jui Ching Hsieh (Apr. 2015). "Design, construction, and preliminary results of a 250-kW organic Rankine cycle system". In: *Applied Thermal Engineering* 80, pp. 339–346. ISSN: 13594311. DOI: 10.1016/j.applthermaleng.2015.01.077.

Georgiadis, Michael, Julio Banga, and Efstratios Pistikopoulos (2011). *Dynamic process modeling*. Wiley-VCH. ISBN: 9783527631339.

Gnielinski, Volker (1975). "Neue Gleichungen für den Wärme- und den Stoffübergang in turbulent durchströmten Rohren und Kanälen". In: *Forschung im Ingenieurwesen A* 41 (1), pp. 8–16. ISSN: 1434-0860. DOI: 10.1007/BF02559682. URL: https://doi.org/10.1007/BF02559682.

Grelet, V., P. Dufour, M. Nadri, T. Reiche, and V. Lemort (July 2015). "Modeling and control of Rankine based waste heat recovery systems for heavy duty trucks". In: *IFAC-PapersOnLine* 28 (8), pp. 568–573. ISSN: 24058963. DOI: 10.1016/j.ifacol.2015.09.028.

Grimison, E.D. (1937). "Correlation and utilization of new data on flow resistance and heat transfer for cross flow of gases over tube banks". In: *Journal of Applied Mechanics*.

Gullapalli, Vijaya Sekhar (2017). "Modeling of brazed plate heat exchangers for ORC systems". In: *Energy Procedia* 129, pp. 443–450. ISSN: 18766102. DOI: 10.1016/j.egypro.2017.09.207.

Haaland, S E (1983). "Simple and Explicit Formulas for the Friction Factor in Turbulent Pipe Flow". In: *Journal of Applied Mechanics*. URL: http://asmedigitalcollection.asme.org/fluidsengineering/article-pdf/105/1/89/5711465/89_1.pdf.

Harvey, Allan H, Christopher W Meyer, Chris D Muzny, and Richard A Perkins (2016). *Thermophysical Properties of Carbon Dioxide and CO 2-Rich Mixtures*. National Institute of Standards and Technology.

Haydary, Juma (2019). *Chemical process design and simulation : Aspen Plus and Aspen Hysys applications*. ISBN: 9781119311447.

Hettiarachchi, H. D. Madhawa, Mihajlo Golubovic, William M. Worek, and Yasuyuki Ikegami (2007). "Optimum design criteria for an Organic Rankine cycle using low-temperature geothermal heat sources". In: *Energy* 32 (9), pp. 1698–1706. ISSN: 03605442. DOI: 10.1016/j.energy.2007.01.005.

Hidayah, Annisa Nurul, Andreas Diga Pratama Putera, and Alison Subiantoro (2020). "Selection of Optimum Working Fluid and Cycle Configuration of Organic Rankine Cycle (ORC) as Bottoming Binary Cycle at Wayang Windu Geothermal Power Plant". In: 'Stanford University. California: '45th Workshop on Geothermal Reservoir Engineering'.

Hung, T C, T Y Shai, and S K Wang (1997). "A REVIEW OF ORGANIC RANKINE CYCLES (ORCs) FOR THE RECOVERY OF LOW-GRADE WASTE HEAT". In: *Energy* 22 (7), pp. 661–667. DOI: 10.1016/S0360-5442(96)00165-X.

Huster, Wolfgang R., Artur M. Schweidtmann, Jannik T. Lüthje, and Alexander Mitsos (2020). "Deterministic global superstructure-based optimization of an organic Rankine cycle". In: *Computers and Chemical Engineering* 141. ISSN: 00981354. DOI: 10.1016/j.compchemeng.2020.106996.

Huster, Wolfgang R., Artur M. Schweidtmann, and Alexander Mitsos (2019). "Impact of Accurate Working Fluid Properties on the Globally Optimal Design of an Organic Rankine Cycle". In: *Computer Aided Chemical Engineering* 47, pp. 427–432. ISSN: 15707946. DOI: 10.1016/B978-0-12-818597-1.50068-0.

Huster, Wolfgang R., Artur M. Schweidtmann, and Alexander Mitsos (2020). "Working fluid selection for organic rankine cycles via deterministic global optimization of design and operation". In: *Optimization and Engineering* 21 (2), pp. 517–536. ISSN: 15732924. DOI: 10.1007/s11081-019-09454-1.

Huster, Wolfgang R., Yannic Vaupel, Adel Mhamdi, and Alexander Mitsos (May 2018). "Validated dynamic model of an organic Rankine cycle (ORC) for waste heat recovery in a diesel truck". In: *Energy* 151, pp. 647–661. ISSN: 03605442. DOI: 10.1016/j.energy.2018.03.058.

Imran, Muhammad, Roberto Pili, Muhammad Usman, and Fredrik Haglind (Oct. 2020). "Dynamic modeling and control strategies of organic Rankine cycle systems: Methods and challenges". In: *Applied Energy* 276. ISSN: 03062619. DOI: 10.1016/j.apenergy.2020.115537.

Jang, Yongtae and Jaeseon Lee (Mar. 2018). "Optimizations of the organic Rankine cycle-based domestic CHP using biomass fuel". In: *Energy Conversion and Management* 160, pp. 31–47. ISSN: 01968904. DOI: 10.1016/j.enconman.2018.01.025.

Jiménez-Arreola, Manuel, Roberto Pili, Christoph Wieland, and Alessandro Romagnoli (2017). "Dynamic study of ORC evaporator operating under fluctuating thermal power from waste heat sources". In: *Energy Procedia* 143, pp. 404–409. ISSN: 18766102. DOI: 10.1016/j.egypro.2017.12.704.

Jiménez-Arreola, Manuel, Christoph Wieland, and Alessandro Romagnoli (May 2019). "Direct vs indirect evaporation in Organic Rankine Cycle (ORC) systems: A comparison of the dynamic behavior for waste heat recovery of engine exhaust". In: *Applied Energy* 242, pp. 439–452. ISSN: 03062619. DOI: 10.1016/j.apenergy.2019.03.011.

Jolevski, Danijel, Ozren Bego, and Petar Sarajcev (2017). "Control structure design and dynamics modelling of the organic Rankine cycle system". In: *Energy* 121, pp. 193–204. ISSN: 03605442. DOI: 10.1016/j.energy.2017.01.007.

Kalina, Jacek and Mateusz Świerzewski (Nov. 2019). "Identification of ORC unit operation in biomass-fired cogeneration system". In: *Renewable Energy* 142, pp. 400–414. ISSN: 18790682. DOI: 10.1016/j.renene.2019.04.080.

Kandlikar, Satish G, Shailesh Joshi, and Shurong Tian (2003). "Effect of Surface Roughness on Heat Transfer and Fluid Flow Characteristics at Low Reynolds Numbers in Small Diameter Tubes". In: *Heat transfer engineering* 24 (3), pp. 4–16. ISSN: 0145-7632.

Khennich, Mohammed and Nicolas Galanis (Feb. 2012). "Optimal design of ORC systems with a low-temperature heat source". In: *Entropy* 14 (2), pp. 370–389. ISSN: 10994300. DOI: 10.3390/e14020370.

Khosravi, A., S. Syri, X. Zhao, and M. E.H. Assad (July 2019). "An artificial intelligence approach for thermodynamic modeling of geothermal based-organic Rankine cycle equipped with solar system". In: *Geothermics* 80, pp. 138–154. ISSN: 03756505. DOI: 10.1016/j.geothermics.2019.03.003.

Koppauer, H., W. Kemmetmüller, and A. Kugi (Nov. 2017). "Modeling and optimal steady-state operating points of an ORC waste heat recovery system for diesel engines". In: *Applied Energy* 206, pp. 329–345. ISSN: 03062619. DOI: 10.1016/j.apenergy.2017.08.151.

Kovacı, Tuğba, Arzu Şencan Şahin, Erkan Dikmen, and Hasan Burak Şavklı (Aug. 2017). "Performance Estimation of Organic Rankine Cycle by Using Soft Computing Technics". In: *International Journal Of Engineering Applied Sciences* 9 (3), pp. 1–10. ISSN: 1309-0267. DOI: 10.24107/ijeas.297737.

Kritzinger, Werner, Matthias Karner, Georg Traar, Jan Henjes, and Wilfried Sihn (Jan. 2018). "Digital Twin in manufacturing: A categorical literature review and classification". In: *IFAC-PapersOnLine* 51 (11), pp. 1016–1022. ISSN: 24058963. DOI: 10.1016/j.ifacol.2018.08.474.

Kuboth, Sebastian, Marc Neubert, Markus Preißinger, and Dieter Brüggemann (2017). "Iterative Approach for the Design of an Organic Rankine Cycle based on Thermodynamic Process Simulations and a Small-Scale Test Rig". In: *Energy Procedia* 129, pp. 18–25. ISSN: 18766102. DOI: 10.1016/j.egypro.2017.09.167.

Kumar, Deepak, Vivek Kumar, and V. P. Singh (Jan. 2013). "Modeling and dynamic simulation of mixed feed multi-effect evaporators in paper industry". In: *Applied Mathematical Modelling* 37 (1-2), pp. 384–397. ISSN: 0307904X. DOI: 10.1016/j.apm.2012.02.039.

Kılıç, Bayram and Emre Arabacı (Jan. 2019). "Alternative approach in performance analysis of organic rankine cycle (ORC)". In: *Environmental Progress and Sustainable Energy* 38 (1), pp. 254–259. ISSN: 19447450. DOI: 10.1002/ep.12901.

Lakhani, Sagar, Appasaheb Raul, and Sandip K. Saha (2017). "Dynamic modelling of ORC-based solar thermal power plant integrated with multitube shell and tube latent heat thermal storage system". In: *Applied Thermal Engineering* 123, pp. 458–470. ISSN: 13594311. DOI: 10.1016/j.applthermaleng.2017.05.115.

Lawless, Jim, Bart Van Campen, and Jim Randle (2020). *Future Geothermal Generation Stack*. Ministry of Business, Innovation & Employment.

Lemmon, Eric, Marcia Huber, and Mark McLinden (Jan. 2013). "NIST Standard Reference Database 23: Reference Fluid Thermodynamic and Transport Properties-REFPROP, Version 9.1". In: URL: https://tsapps.nist.gov/publication/get_pdf.cfm?pub_id=912382.

Li, Shuai, Hongjie Ma, and Weiyi Li (2018). "Dynamic performance analysis of solar organic Rankine cycle with thermal energy storage". In: *Applied Thermal Engineering* 129, pp. 155–164. ISSN: 13594311. DOI: 10.1016/j.applthermaleng.2017.10.021.

Lie, Matthew (2015). "Dynamic Simulation and Control Design for Organic Rankine Cycle Plants". Master's Thesis. University of Auckland.

Liu, Cong, Mingshu Bi, Yihui Zhou, and Guangrui Cui (July 2020). "A novel model for evaporator structural design in the multi-effect evaporation plant". In: *Applied Thermal Engineering* 176. ISSN: 13594311. DOI: 10.1016/j.applthermaleng.2020.115351.

Liu, Liuchen, Yu Pan, Tong Zhu, and Naiping Gao (2017). "Numerical predicting the dynamic behavior of heat exchangers for a small-scale Organic Rankine Cycle". In: *Energy Procedia* 129, pp. 419–426. ISSN: 18766102. DOI: 10.1016/j.egypro.2017.09.127.

Liu, Yingxiang, Wei Ling, Robert Young, and Ming Hsieh (2021). "Deep Learning for Prediction and Fault Detection in Geothermal Operations". In: Workshop on Geothermal Reservoir Engineering. California: Stanford University.

Ljung, Lennart (1998). *System Identification: Theory for the User*. United Kingdom: Pearson Education.

Luo, Xianglong, Yupeng Wang, Junwei Liang, Ji Qi, Wen Su, Zhi Yang, Jianyong Chen, Chao Wang, and Ying Chen (May 2019). "Improved correlations for working fluid properties prediction and their application in performance evaluation of sub-critical Organic Rankine Cycle". In: *Energy* 174, pp. 122–137. ISSN: 03605442. DOI: 10.1016/j.energy.2019.02.124.

Lv, Han, Wei Ting Jiang, and Qun Zhi Zhu (Dec. 2014). "Organic Rankine Cycle Simulation Based on Aspen Plus". In: *Advanced Materials Research* 1070-1072, pp. 1808–1811. DOI: 10.4028/www.scientific.net/amr.1070-1072.1808.

Marchionni, Matteo, Giuseppe Bianchi, Apostolos Karvountzis-Kontakiotis, Apostolos Pesiridis, and Savvas A. Tassou (2017). "Dynamic modeling and optimization of an ORC unit equipped with plate heat exchangers and turbomachines". In: *Energy Procedia* 129, pp. 224–231. ISSN: 18766102. DOI: 10.1016/j.egypro.2017.09.146.

Massimiani, Alessandro, Laura Palagi, Enrico Sciubba, and Lorenzo Tocci (2017). "Neural networks for small scale ORC optimization". In: *Energy Procedia* 129, pp. 34–41. ISSN: 18766102. DOI: 10.1016/j.egypro.2017.09.174.

Mazzi, N., S. Rech, and A. Lazzaretto (Oct. 2015). "Off-design dynamic model of a real Organic Rankine Cycle system fuelled by exhaust gases from industrial processes". In: *Energy* 90, pp. 537–551. ISSN: 03605442. DOI: 10.1016/j.energy.2015.07.083.

McAdams, William H (William Henry) (1954). *Heat transmission*. 3d ed.. McGraw-Hill.

Mert, İlker, Hasan Huseyin Bilgic, Hüseyin Yağlı, and Yıldız Koç (Nov. 2020). "Deep neural network approach to estimation of power production for an organic Rankine cycle system". In: *Journal of the Brazilian Society of Mechanical Sciences and Engineering* 42 (12). ISSN: 18063691. DOI: 10.1007/s40430-020-02701-y.

Meyer, David, Choon Wong, Frithjof Engel, and Susan Krumdieck (2013). *Design and Build of a 1Kilowatt Organic Rankine Cycle Power Generator*.

Ministry for Primary Industries (2020). *Situation and Outlook for Primary Industries (SOPI) December 2020*. URL: www.mpi.govt.nz.

Ministry of Business, Innovation and Employment (2021). *Energy In New Zealand 2021*. Ministry of Business, Innovation and Employment.

Ni, Jiaxin, Li Zhao, Zhengtao Zhang, Ying Zhang, Jianyuan Zhang, Shuai Deng, and Minglu Ma (Mar. 2018). "Dynamic performance investigation of organic Rankine cycle driven by solar energy under cloudy condition". In: *Energy* 147, pp. 122–141. ISSN: 03605442. DOI: 10.1016/j.energy.2018.01.032.

Nur, T. B. and Sunoto (Mar. 2018). "Exergy analysis of biomass organic Rankine cycle for power generation". In: *IOP Conference Series: Materials Science and Engineering* 309 (1). ISSN: 1757899X. DOI: 10.1088/1757-899X/309/1/012057.

Palagi, Laura, Apostolos Pesyridis, Enrico Sciubba, and Lorenzo Tocci (Jan. 2019). "Machine Learning for the prediction of the dynamic behavior of a small scale

ORC system". In: *Energy* 166, pp. 72–82. ISSN: 03605442. DOI: 10.1016/j.energy.2018.10.059.

Pan, Shu Yuan, Mengyao Gao, Kinjal J. Shah, Jianming Zheng, Si Lu Pei, and Pen Chi Chiang (Mar. 2019). "Establishment of enhanced geothermal energy utilization plans: Barriers and strategies". In: *Renewable Energy* 132, pp. 19–32. ISSN: 18790682. DOI: 10.1016/j.renene.2018.07.126.

Peng, Yannan, Xinxing Lin, Jinghang Liu, Wen Su, and Naijun Zhou (Aug. 2021). "Machine learning prediction of ORC performance based on properties of working fluid". In: *Applied Thermal Engineering* 195. ISSN: 13594311. DOI: 10.1016/j.applthermaleng.2021.117184.

Pethurajan, Vignesh, Suresh Sivan, and Grashin C. Joy (June 2018). "Issues, comparisons, turbine selections and applications – An overview in organic Rankine cycle". In: *Energy Conversion and Management* 166, pp. 474–488. ISSN: 01968904. DOI: 10.1016/j.enconman.2018.04.058.

Petrollese, Mario and Daniele Cocco (Dec. 2020). "A multi-scenario approach for a robust design of solar-based ORC systems". In: *Renewable Energy* 161, pp. 1184–1194. ISSN: 18790682. DOI: 10.1016/j.renene.2020.07.120.

Pili, R., S. Eyerer, F. Dawo, C. Wieland, and H. Spliethoff (Dec. 2020). "Development of a non-linear state estimator for advanced control of an ORC test rig for geothermal application". In: *Renewable Energy* 161, pp. 676–690. ISSN: 18790682. DOI: 10.1016/j.renene.2020.07.121.

Pili, Roberto, Hartmut Spliethoff, and Christoph Wieland (Apr. 2017). "Dynamic simulation of an Organic Rankine Cycle - Detailed model of a kettle boiler". In: *Energies* 10 (4). ISSN: 19961073. DOI: 10.3390/en10040548.

Proctor, Matthew J., Wei Yu, Robert D. Kirkpatrick, and Brent R. Young (May 2016). "Dynamic modelling and validation of a commercial scale geothermal organic rankine cycle power plant". In: *Geothermics* 61, pp. 63–74. ISSN: 03756505. DOI: 10.1016/j.geothermics.2016.01.007.

Quaak, P, Van Wijck, and Van Haren (1994). "Comparison of process identification and physical modelling for falling-film evaporators". In: *Food Control* 5 (2), pp. 73–82.

Quoilin, Sylvain, Martijn Van Den Broek, Sébastien Declaye, Pierre Dewallef, and Vincent Lemort (2013). "Techno-economic survey of organic rankine cycle (ORC)

systems". In: *Renewable and Sustainable Energy Reviews* 22, pp. 168–186. ISSN: 13640321. DOI: 10.1016/j.rser.2013.01.028.

Quoilin, Sylvain, Sébastien Declaye, Bertrand F. Tchanche, and Vincent Lemort (2011). "Thermo-economic optimization of waste heat recovery Organic Rankine Cycles". In: *Applied Thermal Engineering* 31 (14-15), pp. 2885–2893. ISSN: 13594311. DOI: 10.1016/j.applthermaleng.2011.05.014.

Rajabloo, Talieh (2017). "Thermodynamic study of ORC at different working and peripheral conditions". In: *Energy Procedia* 129, pp. 90–96. ISSN: 18766102. DOI: 10.1016/j.egypro.2017.09.165.

Rasmussen, Bryan P. (Oct. 2012). "Dynamic modeling for vapor compression systems-Part I: Literature review". In: *HVAC and R Research* 18 (5), pp. 934–955. ISSN: 10789669. DOI: 10.1080/10789669.2011.582916.

Rhinehart, R Russell (2016). *Nonlinear regression modeling for engineering applications : modeling, model validation, and enabling design of experiments*. ISBN: 9781118597972.

Roffel, Brian (2006). *Process Dynamics and Control : Modeling for Control and Prediction*. John Wiley Sons. ISBN: 0470016639.

Russell, Nigel Thomas (1997). "Dynamic Modelling of a Falling-film Evaporator for Model Predictive Control". PhD Thesis. Massey University.

Sansana, Joel, Mark N. Joswiak, Ivan Castillo, Zhenyu Wang, Ricardo Rendall, Leo H. Chiang, and Marco S. Reis (May 2021). "Recent trends on hybrid modeling for Industry 4.0". In: *Computers Chemical Engineering*, p. 107365. ISSN: 00981354. DOI: 10.1016/j.compchemeng.2021.107365. URL: https://linkinghub.elsevier.com/retrieve/pii/S0098135421001435.

Schilling, Johannes, Joachim Gross, and André Bardow (2017). "Integrated design of ORC process and working fluid using process flowsheeting software and PC-SAFT". In: *Energy Procedia* 129, pp. 129–136. ISSN: 18766102. DOI: 10.1016/j.egypro.2017.09.184.

Schweidtmann, Artur M., Wolfgang R. Huster, Jannik T. Lüthje, and Alexander Mitsos (Feb. 2019). "Deterministic global process optimization: Accurate (single-species) properties via artificial neural networks". In: *Computers and Chemical Engineering* 121, pp. 67–74. ISSN: 00981354. DOI: 10.1016/j.compchemeng.2018.10.007.

Seitz, D., O. Gehring, C. Bunz, M. Brunschier, and O. Sawodny (2016). "Dynamic Model of a Multi-Evaporator Organic Rankine Cycle for Exhaust Heat Recovery in Automotive Applications". In: *IFAC-PapersOnLine* 49 (21), pp. 39–46. ISSN: 24058963. DOI: 10.1016/j.ifacol.2016.10.508.

Shah, M. M. (Apr. 1979). "A general correlation for heat transfer during film condensation inside pipes". In: *International Journal of Heat and Mass Transfer* 22 (4), pp. 547–556. ISSN: 0017-9310. DOI: 10.1016/0017-9310(79)90058-9.

Shi, Rongqi, Tianqi He, Jie Peng, Yangjun Zhang, and Weilin Zhuge (May 2016). "System design and control for waste heat recovery of automotive engines based on Organic Rankine Cycle". In: *Energy* 102, pp. 276–286. ISSN: 03605442. DOI: 10.1016/j.energy.2016.02.065.

Sinnott, R K (2005). *Coulson Richardson's chemical engineering. Vol. 6, Chemical engineering design*. Ed. by J M (John Metcalfe) Coulson and J F (John Francis) Richardson. 4th ed.. Includes bibliographical references and index. Oxford : Elsevier Butterworth-Heinemann 2005.

Siwach, Sandeep (2016). "Development and validation of a CFD-based approach towards analysing Pentane vaporizers". PhD Thesis. University of Canterbury.

Soares, Rafael M., Maurício M. Câmara, Thiago Feital, and José Carlos Pinto (Aug. 2019). "Digital Twin for Monitoring of Industrial Multi-Effect Evaporation". In: *Processes* 7 (8), p. 537. ISSN: 2227-9717. DOI: 10.3390/pr7080537.

Sohel, Mohammed Imroz, Susan Krumdieck, Mathieu Sellier, M Imroz Sohel, and Larry J Brackney (2010). *Dynamic Modelling and Simulation of an Organic Rankine Cycle Unit of a Geothermal Power Plant*, pp. 25–29. URL: https://www.researchgate.net/publication/272483115.

Southon, Michael (2015). "Performance and cost evaluation to inform the design and implementation of Organic Rankine Cycles in New Zealand". Master's Thesis. University of Canterbury.

Sun, Jian and Wenhua Li (Aug. 2011). "Operation optimization of an organic rankine cycle (ORC) heat recovery power plant". In: *Applied Thermal Engineering* 31 (11-12), pp. 2032–2041. ISSN: 13594311. DOI: 10.1016/j.applthermaleng.2011.03.012.

Sun, Jie, Qiang Liu, and Yuanyuan Duan (Sept. 2018). "Effects of evaporator pinch point temperature difference on thermo-economic performance of geothermal

organic Rankine cycle systems". In: *Geothermics* 75, pp. 249–258. ISSN: 03756505. DOI: 10.1016/j.geothermics.2018.06.001.

Talybov, Misirkhan A., Lala A. Azizova, and Ilmutdin M. Abdulagatov (Sept. 2019). "Experimental Vapor-Pressures and Derived Thermodynamic Properties of Geothermal Fluids from Baden-Baden Geothermal Field (Southeastern Germany)". In: *Journal of Energy and Power Technology* 1 (4), pp. 1–1. DOI: 10.21926/jept.1904006. URL: https://www.lidsen.com/journals/jept/jept-01-04-006.

Taylor, Leighton John (2015). "Development of a Low Temperature Geothermal Organic Rankine Cycle Standard". Master's Thesis. University of Canterbury.

USDA (2020). *United States Department of Agriculture Foreign Agricultural Service Dairy Production and Trade Developments*.

Wang, Jiangfeng, Zhequan Yan, Man Wang, Maoqing Li, and Yiping Dai (2013). "Multi-objective optimization of an organic Rankine cycle (ORC) for low grade waste heat recovery using evolutionary algorithm". In: *Energy Conversion and Management* 71, pp. 146–158. ISSN: 01968904. DOI: 10.1016/j.enconman.2013.03.028.

Wang, Qi, Weifeng Wu, and Zhilong He (Oct. 2019). "Thermodynamic analysis and optimization of a novel organic Rankine cycle-based micro-scale cogeneration system using biomass fuel". In: *Energy Conversion and Management* 198. ISSN: 01968904. DOI: 10.1016/j.enconman.2019.111803.

Wang, Wei, Shuai Deng, Dongpeng Zhao, Li Zhao, Shan Lin, and Mengchao Chen (Apr. 2020). "Application of machine learning into organic Rankine cycle for prediction and optimization of thermal and exergy efficiency". In: *Energy Conversion and Management* 210. ISSN: 01968904. DOI: 10.1016/j.enconman.2020.112700.

Wang, Xuan, Gequn Shu, Hua Tian, Peng Liu, Dongzhan Jing, and Xiaoya Li (2017). "Dynamic analysis of the dual-loop Organic Rankine Cycle for waste heat recovery of a natural gas engine". In: *Energy Conversion and Management* 148, pp. 724–736. ISSN: 01968904. DOI: 10.1016/j.enconman.2017.06.014.

Wei, Donghong, Xuesheng Lu, Zhen Lu, and Jianming Gu (2007). "Performance analysis and optimization of organic Rankine cycle (ORC) for waste heat recovery". In: *Energy Conversion and Management* 48 (4), pp. 1113–1119. ISSN: 01968904. DOI: 10.1016/j.enconman.2006.10.020.

Wei, Donghong, Xuesheng Lu, Zhen Lu, and Jianming Gu (2008). "Dynamic modeling and simulation of an Organic Rankine Cycle (ORC) system for waste heat

recovery". In: *Applied Thermal Engineering* 28 (10), pp. 1216–1224. ISSN: 13594311. DOI: 10.1016/j.applthermaleng.2007.07.019.

Wu, Peiyi and W A Little (1984). "Measurement of the heat transfer characteristics of gas flow in fine channel heat exchangers used for microminiature refrigerators". In: *Cryogenics* 24 (8), pp. 415–420. ISSN: 0011-2275. DOI: https://doi.org/10.1016/0011-2275(84)90015-8. URL: https://www.sciencedirect.com/science/article/pii/0011227584900158.

Xu, Bin, Dhruvang Rathod, Shreyas Kulkarni, Adamu Yebi, Zoran Filipi, Simona Onori, and Mark Hoffman (2017). "Transient dynamic modeling and validation of an organic Rankine cycle waste heat recovery system for heavy duty diesel engine applications". In: *Applied Energy* 205, pp. 260–279. ISSN: 03062619. DOI: 10.1016/j.apenergy.2017.07.038.

Xu, Bin, Dhruvang Rathod, Adamu Yebi, Simona Onori, Zoran Filipi, and Mark Hoffman (Jan. 2020). "A comparative analysis of dynamic evaporator models for organic Rankine cycle waste heat recovery systems". In: *Applied Thermal Engineering* 165. ISSN: 13594311. DOI: 10.1016/j.applthermaleng.2019.114576.

Yadav, Drishti and Om Prakash Verma (July 2020). "Energy optimization of Multiple Stage Evaporator system using Water Cycle Algorithm". In: *Heliyon* 6 (7). ISSN: 24058440. DOI: 10.1016/j.heliyon.2020.e04349.

Yan, Dong, Fubin Yang, Fufang Yang, Hongguang Zhang, Zhiyu Guo, Jian Li, and Yuting Wu (July 2021). "Identifying the key system parameters of the organic Rankine cycle using the principal component analysis based on an experimental database". In: *Energy Conversion and Management* 240, p. 114252. ISSN: 01968904. DOI: 10.1016/j.enconman.2021.114252. URL: https://linkinghub.elsevier.com/retrieve/pii/S0196890421004283.

Yang, Fubin, Heejin Cho, Hongguang Zhang, Jian Zhang, and Yuting Wu (May 2018). "Artificial neural network (ANN) based prediction and optimization of an organic Rankine cycle (ORC) for diesel engine waste heat recovery". In: *Energy Conversion and Management* 164, pp. 15–26. ISSN: 01968904. DOI: 10.1016/j.enconman.2018.02.062.

Yin, Shen, Steven X. Ding, Xiaochen Xie, and Hao Luo (2014). "A review on basic data-driven approaches for industrial process monitoring". In: *IEEE Transactions on Industrial Electronics* 61 (11), pp. 6418–6428. ISSN: 02780046. DOI: 10.1109/TIE.2014.2301773.

Young, Brent R (1992). "Modelling and Identification of a Climbing Film Evaporator". PhD Thesis. University of Canterbury.

Yu, Wei, Panos Patros, Brent Young, Elsa Klinac, and Timothy Gordon Walmsley (June 2022). "Energy digital twin technology for industrial energy management: Classification, challenges and future". In: *Renewable and Sustainable Energy Reviews* 161. ISSN: 18790690. DOI: 10.1016/j.rser.2022.112407.

Zhang, Jianhua, Wenfang Zhang, Guolian Hou, and Fang Fang (Sept. 2012). "Dynamic modeling and multivariable control of organic Rankine cycles in waste heat utilizing processes". In: *Computers and Mathematics with Applications* 64 (5), pp. 908–921. ISSN: 08981221. DOI: 10.1016/j.camwa.2012.01.054.

Zhang, Jianhua, Yeli Zhou, Rui Wang, Jinliang Xu, and Fang Fang (Mar. 2014). "Modeling and constrained multivariable predictive control for ORC (Organic Rankine Cycle) based waste heat energy conversion systems". In: *Energy* 66, pp. 128–138. ISSN: 03605442. DOI: 10.1016/j.energy.2014.01.068.

Zhang, Ying, Shuai Deng, Li Zhao, Shan Lin, Mengjie Bai, Wei Wang, and Dongpeng Zhao (Apr. 2019). "Dynamic test and verification of model-guided ORC system". In: *Energy Conversion and Management* 186, pp. 349–367. ISSN: 01968904. DOI: 10.1016/j.enconman.2019.02.055.

Zhao, Rui, Hongguang Zhang, Songsong Song, Yaming Tian, Yuxin Yang, and Yi Liu (Jan. 2018). "Integrated simulation and control strategy of the diesel engine–organic Rankine cycle (ORC) combined system". In: *Energy Conversion and Management* 156, pp. 639–654. ISSN: 01968904. DOI: 10.1016/j.enconman.2017.11.078.

Zhi, Liang Hui, Peng Hu, Long Xiang Chen, and Gang Zhao (Jan. 2019). "Multiple parametric analysis, optimization and efficiency prediction of transcritical organic Rankine cycle using trans-1,3,3,3-tetrafluoropropene (R1234ze(E)) for low grade waste heat recovery". In: *Energy Conversion and Management* 180, pp. 44–59. ISSN: 01968904. DOI: 10.1016/j.enconman.2018.10.086.